HHS Public Access

Author manuscript

Nat Med. Author manuscript; available in PMC 2021 April 01.

Published in final edited form as:

Nat Med. 2020 April ; 26(4): 519–528. doi:10.1038/s41591-020-0782-y.

CTLA-4 and PD-1 dual blockade induces SIV reactivation without control of rebound after ART interruption

Justin Harper[1], **Shari Gordon**[2,3], **Chi Ngai Chan**[4], **Hong Wang**[1], **Emily Lindemuth**[5], **Cristin Galardi**[3,6], **Shane D. Falcinelli**[3], **Samuel L.M. Raines**[3], **Jenna L. Read**[3], **Kevin Nguyen**[1], **Colleen S McGary**[1], **Michael Nekorchuk**[4], **Kathleen Busman-Sahay**[4], **James Schawalder**[3,6], **Colin King**[1], **Maria Pino**[1], **Luca Micci**[1], **Barbara Cervasi**[1], **Sherrie Jean**[7], **Andrew Sanderson**[8], **Brian Johns**[2,3], **A. Alicia Koblansky**[3,6], **Heather Amrine-Madsen**[3,6], **Jeffrey Lifson**[9], **David M. Margolis**[3], **Guido Silvestri**[1,10], **Katharine J Bar**[5], **David Favre**[2,3], **Jacob D. Estes**[4,11], **Mirko Paiardini**[*,1,10,12]

[1]Division of Microbiology and Immunology, Yerkes National Primate Research Center, Emory University, Atlanta, Georgia, USA.

[2]HIV Discovery Performance Unit, GlaxoSmithKline, Research Triangle Park, North Carolina, USA.

[3]UNC HIV Cure Center and Department of Medicine, University of North Carolina at Chapel Hill, Chapel Hill, North Carolina, USA.

[4]Vaccine and Gene Therapy Institute, Oregon Health & Science University, Beaverton, Oregon, USA.

[5]Perelman School of Medicine, University of Pennsylvania, Philadelphia, Pennsylvania, USA.

[6]HIV Discovery, ViiV Healthcare, Research Triangle Park, North Carolina, USA.

[7]Division of Animal Resources, Yerkes National Primate Research Center, Emory University, Atlanta, Georgia, USA.

[8]Biopharm Innovation, GlaxoSmithKline, Stevenage, UK.

[*]**Corresponding Author:** Dr. Mirko Paiardini; mirko.paiardini@emory.edu.

Author Contributions

J.H. contributed to conceptualization, methodology, formal analysis, investigation, writing – original draft, writing – review & editing, and visualization; S.G. contributed to conceptualization, formal analysis, investigation, and writing – original draft; C.N.C. contributed to formal analysis, investigation, and visualization; H.W. contributed to investigation; E.L. contributed to formal analysis and investigation; C.G. contributed to investigation; S.D.F. contributed to methodology and investigation; S.L.M.R. contributed to investigation; J.L.R. contributed to investigation; K.N. contributed to investigation; C.S.M. contributed to conceptualization and investigation; M.N. contributed to investigation; K.B.-S. contributed to investigation; J.S. contributed to formal analysis and investigation; C.K. contributed to investigation; M.P. contributed in investigation; L.M. contributed to investigation; B.C. contributed to investigation; S.J. contributed to investigation; A.S. contributed to investigation; B.J. contributed to resources; A.A.K. contributed to investigation; H.A.-M. contributed to methodology and writing – review & editing; J.L. contributed to methodology and writing – review & editing; D.M.M. contributed to methodology, resources, writing – review & editing, and funding acquisition; G.S. contributed to writing – review & editing and funding acquisition; K.J.B. contributed to methodology, formal analysis, and writing – review & editing; D.F. contributed to conceptualization, methodology, resources, writing – review & editing, supervision, and funding acquisition; J.D.E. contributed to methodology and writing – review & editing; and M.P. contributed to conceptualization, methodology, resources, writing – original draft, writing – review & editing, supervision, and funding acquisition.

Competing Interests Statement

The authors declare the following conflict of interest: S.G., C.G. J.S., A.S., B.J., A.A.K., H.A.-M., and D.F. are employed by and/or have financial interests in GlaxoSmithKline or ViiV Healthcare

[9]AIDS and Cancer Virus Program, Frederick National Laboratory for Cancer Research, Frederick, Maryland, USA.

[10]Department of Pathology and Laboratory Medicine, Emory University School of Medicine, Atlanta, Georgia, USA.

[11]Oregon National Primate Research Center, Oregon Health & Science University, Beaverton, Oregon, USA.

[12]Lead Contact

Abstract

The primary HIV reservoir is composed of resting memory CD4$^+$ T-cells, which often express the immune checkpoint receptors PD-1 and CTLA-4 that limit T-cell activation via synergistic mechanisms. Using SIV-infected, long-term anti-retroviral therapy (ART)-treated rhesus macaques, we demonstrate that PD-1, CTLA-4, and dual CTLA-4/PD-1 immune checkpoint blockade (ICB) using monoclonal antibodies is well-tolerated with evidence of bioactivity in blood and lymph nodes. Dual blockade was remarkably more effective than PD-1 blockade alone in enhancing T-cell cycling and differentiation; expanding effector-memory T-cells; and inducing robust viral reactivation in plasma and PBMCs. In lymph node, dual CTLA-4/PD-1 blockade, but not PD-1 alone, decreased total and intact SIV-DNA in CD4$^+$ T-cells, and SIV-DNA and -RNA in B-cell follicles, a major site of viral persistence during ART. None of the tested interventions enhanced SIV-specific CD8$^+$ T-cell responses during ART or viral control after ART interruption. Thus, despite CTLA-4/PD-1 blockade inducing robust latency reversal and reducing total levels of integrated virus, the degree of reservoir clearance was still insufficient to achieve viral control. These results suggest that ICB regimens targeting PD-1 and/or CTLA-4, if performed in people living with HIV with sustained aviremia, are unlikely to induce HIV remission in the absence of additional interventions.

Introduction

Due to the complexity and diversity of the CD4$^+$ T-cell compartment, the identification of the specific subsets that preferentially harbor replication competent SIV/HIV under long-term anti-retroviral therapy (ART) is considered a critical step to facilitate the design of therapeutics aimed at eliminating persistent viral reservoirs. Recent studies reported high levels of viral DNA in memory CD4$^+$ T-cells expressing immune checkpoint receptors (ICR)[1-3], including programmed cell death protein 1 (PD-1) and cytotoxic T-lymphocyte-associated protein 4 (CTLA-4), which define a quiescent population with impaired effector function enforced by distinct, synergistic pathways[4,5]. Lymph node (LN) CD4$^+$PD-1$^+$ T-cells, in particular follicular helper T-cells (T_{FH}) in the B-cell follicle (BCF), represent a major potential source of inducible, replication competent virus in ART-treated, HIV-infected subjects[2,6]. Chronic viral infection enhances PD-1 expression on HIV-specific CD8$^+$ T-cells, which exhibit impaired cytokine production upon antigen stimulation, diminished proliferative capacity, abnormal cellular differentiation, and exhaustion[7,8]. In rhesus macaques (RMs) we have demonstrated that, in addition to PD-1$^+$ T_{FH} cells, memory CD4$^+$CTLA-4$^+$PD-1$^-$ T-cells harbor replication-competent SIV; phenotypically overlap with

regulatory T-cells (T_{REGS}); reside in the lymphoid T-cell zone (TCZ); and increase their contribution to the viral reservoir over time with ART[1]. Collectively, these observations provide strong rationale for targeting CTLA-4/PD-1-expressing T-cells with the aim of relieving ("shock") the quiescent transcriptional state that promotes viral latency while also restoring immune effector functions that may result in viral clearance ("kill").

As a proof of concept in ART-treated, HIV-infected patients, the sequential *in vivo* blockade of CTLA-4[9] and PD-1[10] yielded greatly expanded levels of cell-associated HIV-RNA in a patient with metastatic melanoma; furthermore, PD-1 blockade produced significant declines in HIV-DNA in a patient with relapsed non-small-cell lung cancer[11], but has proven highly variable.[10,12,13] In viremic, SIV-infected RMs (without ART or with viremia incompletely suppressed by ART), CTLA-4 blockade has produced inconsistent results on viral reactivation and on SIV-specific $CD8^+$ T-cells responses[14,15]. Similarly, PD-1 blockade decreased set point viremia and improved SIV-specific T-cell responses during chronic infection[16] with only a modest effect in enhancing antiviral responses during short-term ART[17] and no impact upon long-term ART[18]. In this study we examined, for the first time, the immunologic and virologic effects, and therapeutic potential of PD-1 and CTLA-4 blockade in SIV-infected RMs treated with long-term ART.

Results

CTLA-4 and PD-1 blockade is biologically active in SIV-infected, ART-treated RMs.

Thirty-four RMs were intravenously infected with SIV_{mac239} (Fig. 1a); RFf16 was euthanized at day 25 post-infection (d25 p.i.) related to rapid AIDS progression. Set point viral loads ranged between $2.5x10^5$-$8.4x10^7$ copies/mL with one outlier, RKt16 at $8x10^2$ copies/mL. At d60 p.i. ART consisting of tenofovir (TDF), dolutegravir (DTG), and emtricitabine (FTC) was initiated and maintained for up to 13.5 months. Viremia was controlled to undetectable levels (<60 copies/mL) with transient blips observed in RAi16, ROp16, and RZl16 (Extended Data Fig. 1 and Extended Data Fig. 2a). RMs were stratified into treatment groups based on acute ("peak") and set point ("chronic" at ART initiation) viral load; duration of virologic suppression; MHC haplotype (6 *Mamu*-A*01^+); and the lack of naturally arising, cross-reactive anti-drug antibodies (ADAs) against the therapeutic ICB monoclonal antibodies (mAb) in plasma (Supplementary Fig. 1 and Supplementary Table 1). Four doses of mAbs targeting PD-1 and/or CTLA-4 were infused weekly. RMs had an average of 181.4 ± 4.9 days of virologic suppression, ensuring that immune interventions and SIV-DNA reservoir measurements were not conducted in the setting of overt viral replication. Two-weeks after mAb administrations, all animals underwent ART analytical therapy interruption (ATI) and were followed for 7 months.

In non-human primates (NHPs), repeated doses of ipilimumab, a humanized IgG1 anti-CTLA-4 mAb, did not induce ADAs[14,15]; however, nivolumab, a humanized IgG4 anti-PD-1 mAb, was immunogenic with blunted proliferative responses upon serial administration[19]. To improve the effective dosing duration, an IgG4 nivolumab-biosimilar anti-PD-1 was rhesusized with human variable domains and macaque constant regions (αPD-1, n=6), and further formulated as a bispecific IgG1 mAbdAb with ipilimumab-biosimilar anti-CTLA-4 mAb (BsAb, n=8). Additional treatment groups include ipilimumab-biosimilar anti-CTLA-4

mAb (αCTLA-4, n=6) with Fc-γ binding activity; anti-CTLA-4 mAb in conjunction with an anti-PD-1 mAb (combined blockade, n=7); and a control mAbdAb (VHDUM), which lacks known specificity (control, n=6; Extended Data Fig. 2b).

Infusion resulted in sustained plasma concentrations of all mAbs through four cycles of administration (Extended Data Fig. 3a); yet, the BsAb formulation had faster *in vivo* clearance. Few animals showed the emergence of ADAs, which were associated with a reduction in plasma mAb concentrations (Extended Data Fig. 3b). Target receptor engagement was remarkably high, both for memory ($CD95^+$) $CD4^+$ and $CD8^+$ T-cells, as confirmed via PD-1 occupancy using the EH12.2H7 detection antibody in peripheral blood mononuclear cells (PBMCs; Fig. 1b,c,d; Supplementary Fig. 2) and LN biopsies (Fig. 1e,f,g); however, BsAb treatment was associated with reduced PD-1 occupancy by d21 post-treatment (p.t.), consistent with its pharmacokinetics (Extended Data Fig. 3a). PD-1 occupancy was observed within LN-resident T_{FH} ($PD\text{-}1^{hi}CXCR5^+CD95^+CD4^+$ T-cells) indicative of follicular distribution, without impacting follicle homing as measured by CXCR5 expression (Fig. 1h, data not shown)[20]. Thus, the tested mAbs engage their cognate receptor in blood and LN; whereas, the BsAb failed to improve plasma concentrations or target engagement as compared to combined blockade.

Mono- and dual-ICB were well-tolerated without evidence of treatment-induced clinical pathology, acute inflammatory reactions, cytokine release syndrome, abnormal blood counts, nephrotoxicity, or hepatotoxicity (Supplementary Table 2; Supplementary Fig. 3a,b,c). None of the treatment regimens impacted the number of circulating neutrophils or eosinophils, while αPD-1 exhibited a transient increase in the number of monocytes (Supplementary Fig. 3d). Immunophenotypic analysis of unoccupied PD-1 epitopes (clone 913429) in LN demonstrated that PD-1 blockade did not result in an expansion or contraction of $PD\text{-}1^+$ T-cells (data not shown) or T_{FH} (Supplementary Fig. 4a,b). CTLA-4 blockade, particularly in combination with PD-1 blockade, was associated with an expansion of $CTLA\text{-}4^+$memory $CD4^+$ T-cells in PBMCs and LN (Supplementary Fig. 4c,d), and significantly increased levels of $CD4^+$ regulatory T-cells (T_{REGS}; $CD25^+CD127^-FoxP3^+$) in peripheral blood (PB) and LN (Fig. 1i,j). Furthermore, the magnitude of the $CD4^+$ T_{REG} expansion at day 28 p.t. was directly correlated with the plasma concentration of CTLA-4 blocking mAbs ($r=0.5692$, $p=0.0434$; Supplementary Fig. 4e). Therefore, dual CTLA-4/PD-1 blockade was biologically active and demonstrated an acceptable safety profile in ART-treated, SIV-infected RMs.

T-cell proliferative and effector responses are synergistically improved by dual CTLA-4/PD-1 blockade

As ICB was biologically active, we determined how those interventions impacted the levels of proliferating T-cells. Blockade of CTLA-4, particularly when combined with PD-1 blockade, was remarkably effective in expanding the number of circulating memory $CD4^+$ T-cells expressing Ki-67. Specifically, combined blockade induced a large increase in the number of PB memory $CD4^+Ki\text{-}67^+$ T-cells (from 106.3 ± 9.263 to 642.6 ± 80.04 at d7 p.t.; Fig. 2a,b) and PB memory $CD8^+Ki\text{-}67^+$ T-cells (from 71.43 ± 24.66 to 212.3 ± 54.96 at d14 p.t.; Fig. 2c,d). Increased T-cell cycling induced by CTLA-4 blockade alone, and more significantly in combination with PD-1 blockade, was coupled with a marked expansion of

circulating effector-memory T-cells (T_{EM}, $CCR7^{-}CD95^{+}$). With a full treatment cycle, the number of T_{EM} increased from 111.9 ± 13.52 to 457.0 ± 66.30 cells/μL ($p<0.0001$) for $CD4^{+}$ T-cells and from 446.0 ± 165.5 to 781.4 ± 196.9 cells/μL for $CD8^{+}$ T-cells ($p=0.0130$; Fig. 2e,f) with combined blockade, while those levels remain virtually unchanged in controls or after αPD-1 monotherapy. Therefore, dual CTLA-4/PD-1 blockade exhibited strong synergy in enhancing the number of T_{EM} and proliferative responses in PB.

In lymphoid tissue, CTLA-4 blockade enhanced Ki-67 expression in memory $CD4^{+}$ T-cells (αCTLA-4, $p=0.0125$; BsAb, $p=0.0137$; combined blockade, $p<0.0001$; Fig. 2g); $CD4^{+}$ T_{EM} (Fig. 2h); and memory $CD8^{+}$ T-cells (BsAb, $p=0.0235$; combined blockade, $p=0.0009$; Fig. 2i). Dual blockade also uniquely increased activation ($HLA\text{-}DR^{+}CD38^{+}$) of both memory $CD4^{+}$ (combined blockade, $p=0.0082$; BsAb, $p=0.0200$; Fig. 2j) and $CD8^{+}$ T-cells (combined blockade, $p=0.0221$; Fig. 2k). Only dual blockade produced an increase in the frequency of $CXCR3^{+}$ T_{FH}, which produce IFN-γ and provide B-cell help for IgG production (combined blockade, $p=0.0047$; BsAb, $p=0.0426$; Fig. 2l)[21]. Therefore, combined blockade results in increased T-cell activation and cell cycling, suggesting treatment may enhance viral reactivation and/or viral clearance.

SIV-specific $CD8^{+}$ T-cell responses are not improved by blockade of PD-1 and/or CTLA-4 during long-term ART

Blockade of CTLA-4 and PD-1 signaling is predicted to improve the function of exhausted cytotoxic T lymphocytes (CTL; i.e. “kill”). Immunophenotypic analysis revealed that dual blockade increased the frequency of granzyme B expression in LN $CTLA\text{-}4^{+}PD\text{-}1^{+}$ and $CTLA\text{-}4^{+}PD\text{-}1^{-}$ subsets of memory $CD8^{+}$ T-cells (Extended Data Fig. 4a,b). Following CellTrace labeling and T-cell receptor stimulation, combined blockade leads to a reduction of non-dividing $CD4^{+}$ T-cells at d21 p.t. ($p=0.0463$), with a less pronounced effect within $CD8^{+}$ T-cells (Supplementary Fig. 5a,b,c,d). Prior to therapy, SIV-specific memory $CD8^{+}$ T-cells, as determined via Gag-CM9 tetramer staining, were enriched in PD-1 and eomesodermin (EOMES), a T-box transcription factor that regulates T-cell exhaustion[22,23] (Extended Data Fig. 5a,b). ICB failed to substantially expand the frequency of SIV-specific memory $CD8^{+}$ T-cells in LN and PBMCs (Extended Data Fig. 6a,b) or to significantly enhance markers of activation, proliferation, or cytolytic responses (Extended Data Fig. 5c,d,e,f,g,h,i,j). By ELISpot analyses in PBMCs and LN, none of the interventions increased IFN-γ production in response to SIV-Gag (Extended Data Fig. 6c,d) or SIV-Env peptide stimulation (Supplementary Fig. 6a,b). Furthermore, αCTLA-4 monotherapy resulted in a significant fold change reduction in SIV-Gag-stimulated IFN-γ responses in PBMCs ($p=0.0411$; Extended Data Fig. 6c) and a cross-sectional decrease in the SIV-Env-stimulated IFN-γ response in LN (Supplementary Fig. 6b). Finally, ICB failed to impact the frequency of PB memory T-cells co-expressing IL-2, IFN-γ, TNFα, and/or CD107a following *ex vivo* SIV-Gag (Extended Data Fig. 6e,f) or -Env peptide stimulation (Supplementary Fig. 6c,d). In SIV-Gag peptide responding T-cells, defined as those expressing either IFN-γ, IL-2, TNFα, or CD107a, therapies incorporating CTLA-4 blockade significantly increased the frequency of proliferating memory $CD4^{+}$ T-cells relative to baseline (αCTLA-4, $p=0.0109$; combined blockade, $p=0.0068$) and combined blockade alone enhanced the proliferation of memory $CD8^{+}$ T-cells relative to controls ($p=0.0259$) (Supplementary Fig. 6e,f). Overall,

these findings indicated that ICB is insufficient to enhance SIV-specific responses when performed in the context of long-term ART suppression.

CTLA-4 and PD-1 combined blockade induces robust viral reactivation in ART-treated, SIV-infected RMs

By promoting cell cycling, ICB is proposed to function as a latency reversing agent (LRA) by increasing viral transcription[24]. Longitudinal quantification of plasma viral loads demonstrated detectable viral RNA on-ART in a fraction of RMs across all interventions (Fig. 3a,b,c,d,e). Enhanced viral reactivation was observed for both co-blockades as compared to monotherapies, stratified either by animal or by the number of detectable events (Fig. 3f). In particular, combined blockade enhanced both the frequency (57.1% of RMs and 32.1% of events) and magnitude (average: $9.1x10^2$ SIV-RNA copies/mL) of detectable plasma SIV-RNA relative to controls (0% of events), αPD-1 (12.5% of events; $7.2x10^2$ SIV-RNA copies/mL), and αCTLA-4 monotherapy (12.5% of events; $7.1x10^2$ SIV-RNA copies/mL), thus suggesting a synergistic effect of blocking PD-1 and CTLA-4 in reversing viral latency. Furthermore, measurable virus induction after ICB monotherapy skewed toward later treatments, with 66.7% of reactivation events occurring after the third infusion, while both dual blockade strategies produced 66.7% of their reactivation events before the third infusion. As expected based on the early loss of PD-1 occupancy, the BsAb group produced fewer unique reactivation events following the third infusion as compared to combined blockade. The propensity towards viral reactivation was directly associated with the set point plasma viral load (p=0.0038; Fig. 3g, Extended Data Fig. 1), but not with peak viral load or the size of SIV reservoir during suppressive ART (data not shown). Of note, only combined blockade yielded enhanced levels of cell-associated SIV-RNA in PBMCs following the first (d7 p.t.) and fourth infusion (d28 p.t.) as compared to baseline (p=0.0156; p=0.0156; Fig. 3h). Although with some heterogeneity between individual animals, dual CTLA-4/PD-1 blockade acts as a synergistic, latency-reversing intervention that induces robust levels of viral reactivation.

CTLA-4 and dual blockade, but not PD-1 blockade, reduces the total and intact SIV-DNA in LN

To determine the impact of ICB-induced viral reactivation and effector cell expansion on viral persistence, we longitudinally measured the levels of cell-associated SIV-DNA with qPCR. In PBMCs, ICB did not impact viral DNA content (Extended Data Fig. 7a), but combined blockade increased the transcriptional ratio of SIV-RNA to SIV-DNA (p=0.0313; p=0.0156; Extended Data Fig. 7b), consistent with induction of viral expression. Mononuclear cells derived from LN, a major site of viral persistence[25], were sorted for memory $CD4^+$ T-cell subsets: T_{FH} ($PD\text{-}1^+CD200^{hi}$), T_{REG} ($CD25^+CD127^-$), central-memory (T_{CM}; $CCR7^+$), and effector-memory (T_{EM}; $CCR7^-$; Fig. 4a). Importantly, CTLA-4 blockade, whether as mono- or combination therapy, significantly decreased cell-associated SIV-DNA in T_{EM} (αCTLA-4, p=0.0031; combined blockade, p=0.0044; BsAb, p=0.0147; Fig. 4b). The preferential reduction of SIV-DNA within the T_{EM} compartment is consistent with the observation that this subset is the most affected in terms of cell cycling by combined blockade (Fig. 2h), perhaps suggesting the depletion of cycling cells in which SIV-RNA production was reactivated.

To assess if therapy-mediated reductions in total SIV-DNA translated into a functional decrease in intact virus, we assayed for integrated viral genomes in LN $CD4^+$ cells using the intact proviral DNA assay (IPDA)[26]. The intact reservoir was remarkably stable in controls and with anti-PD-1 monotherapy (controls, 1458 ± 475.4 to 1646 ± 424.5; αPD-1, 1448 ± 300.6 to 1514 ± 295.4 intact proviral genomes per 10^6 $CD4^+$ cells, d-29 and d28 p.t., respectively). In comparison, all CTLA-4 blockades result in a fold change reduction in the frequency of intact provirus (Extended Data Fig. 7c,d), which was most pronounced, relative to baseline, for dual CTLA-4/PD-1 blockade (combined blockade, p=0.0860; BsAb, p=0.0255; Fig. 4c; representative data shown in Extended Data Fig. 7e).

To define the anatomic localization of SIV-RNA^+ cells in LN, we employed RNAscope, an *in situ* hybridization assay to detect and quantify cells harboring SIV-RNA ($vRNA^+$) by tissue location[27]. Only combined blockade showed a significant reduction in the number of $vRNA^+$ cells normalized per 10^5 cellular nuclei as compared to baseline (p=0.0312; Extended Data Fig. 8a), which was confirmed specifically within the BCF (p=0.0312; Fig. 4d,e), and not within the TCZ or the medullary cords (not shown). The decline in BCF-resident $vRNA^+$ cells in combination with heightened proliferative capacity in LN memory $CD4^+$ T-cells (Fig. 2g), suggests that combined blockade has the potential to target and reduce a subset of cells undergoing viral reactivation. Finally, only BsAb-treated RMs showed a measurable decrease in $vDNA^+$ cells, quantified by DNAscope and normalized per 10^5 cells, in the BCF (p=0.0391; Fig. 4f) and TCZ (p=0.0156; Fig. 4g; representative images shown in Fig. 4h), and treatment did not differentially impact T-cell or macrophage viral reservoirs (Extended Data Fig. 8b,c,d). As a caveat, DNAscope cannot distinguish between defective and intact viral genomes; however, we did observe a correlation between the reservoir content as determined by IPDA and DNAscope following therapy (Extended Data Fig. 8e). Collectively, these results highlight that, in lymphoid tissue, combined blockade limits SIV reservoir content within $CD4^+$ T_{EM} concomitant with reduced viral production and persistence in the BCF, suggesting a direct link between viral reactivation and clearance in a fraction of infected cells.

Dual CTLA-4/PD-1 blockade does not control or delay viral rebound after ATI

To functionally assess the impact of ICB on the size of the viral reservoir we conducted an ATI two weeks after ICB cessation. Overall, there was a limited impact on delaying viral rebound, with αPD-1 treatment (p=0.0390) and dual CTLA-4/PD-1 blockade producing a slight delay in time to measurable viral rebound as compared to controls (control, 7.67 ± 0.82 days; αCTLA-4, 8.00 ± 0.52 days; αPD-1, 12.83 ± 2.04 days; combined blockade 10.29 ± 1.69 days; BsAb, 12.75 ± 3.48 days; Extended Data Fig. 9a,b,c,d,e,f). 12 of 13 RMs with prior ICB-mediated viral reactivation re-established undetectable plasma viremia between their terminal on-ART reactivation event and the first post-ATI observation, consistent with the observed on-ART viremia being LRA mediated and not a failure of the ART regimen. All blockades failed to significantly attenuate the set point plasma viral load post-ATI (Extended Data Fig. 9g); the fold change in peak viremia relative to acute infection (not shown); and the fold change in set point viremia at necropsy (d170 post-ATI) relative to chronic infection (d52 p.i.; Extended Data Fig. 9h) as compared to controls. Furthermore, ICB failed to impact on cell-associated SIV-DNA or -RNA levels, or their respective ratio in

axillary LN or spleen at necropsy (Extended Data Fig. 9i; Supplementary Fig. 7). Of note, post-ATI viremia was associated with a robust induction of proliferation, activation, and CTL functionality in SIV-specific memory $CD8^+$ T-cells relative to during ART, suggesting a critical dependence on sufficient antigen burdens (Extended Data Fig. 5g,h,i,j). Thus, the potent latency reversal and the partial reduction of the viral reservoir induced by combined CTLA-4 and PD-1 blockade under long-term ART is insufficient, alone, to control viral rebound after ART interruption.

Finally, single genome sequencing of gp160 *env* was performed on plasma during on-ART, ICB-mediated viral reactivation (n=8) and at rebound following ATI (n=8). Qualitatively, all RMs across ICB treatments yielded a similar number of viral lineages during rebound (3-10 lineages; Fig. 3i) consistent with a polyclonal nature of the seeded, latent viral reservoir and rebound virus[28]. Only αPD-1 monotherapy was associated with highly restricted clonality in reactivating virus (i.e. a single lineage); whereas, virus arising from αCTLA-4 monotherapy (2-7 lineages) and dual blockade (combined blockade, 5-7 lineages; BsAb, 4-7 lineages) were polyclonal in nature (Fig. 3i; Extended Data Fig. 10). These data suggest that combination CTLA-4/PD-1 blockade was able to reactivate a larger and more diverse latent reservoir as compared to αPD-1 monotherapy (Supplementary Table 3).

Discussion

The quest for a functional cure for HIV is hampered by a limited understanding of the mechanisms underlying the long-term persistence of HIV reservoirs, including both latently and actively infected cells; the absence of reliable biomarkers for the selective targeting of latently infected cells; the lack of potent LRAs that induce robust viral reactivation during suppressive ART; and the inhibition of HIV-specific cytotoxic T-cell responses mediated by co-inhibitory signaling arising from chronic immune activation. The results of the current study indicate that CTLA-4 blockade, particularly when combined with PD-1 blockade, enhances activation, proliferation, and expansion of LN and PB memory $CD4^+$ and $CD8^+$ T-cells, including T_{EM} cells. In contrast, anti-PD-1 monotherapy showed limited effects on reversing the negative regulation of T-cell activation. Of note, combined blockade potently enhanced viral reactivation on-ART as measured by plasma viremia, among the most persistent published to date, and increased levels of cell-associated SIV-RNA in PBMCs. Furthermore, RMs receiving combined CTLA-4/PD-1 blockade showed a greater number of reactivated viral lineages compared to anti-PD-1 monotherapy. These findings suggest that blocking CTLA-4 co-inhibitory signaling, especially in combination with PD-1 blockade, is critical to reverse latency in a larger subset of memory $CD4^+$ T-cells during long-term ART.

Although combined blockade-induced proliferation provided an effective “shock” to break viral latency in memory $CD4^+$ T-cells, this treatment, as well as the αCTLA-4 and αPD-1 monotherapies, failed to induce a significant functional reversal of exhaustion. Previous *in vivo* PD-1 blockades in SIV-infected RMs have demonstrated marked enhancement of SIV-specific anti-viral responses; however, they were conducted in the absence of ART[16,29,30] and either before ART initiation or during short-term ART with detectable viral loads[17,29,31], suggesting that the presence of antigen at the time of PD-1 blockade is important for breaking the exhausted phenotype. Consistently, PD-1 blockade failed to

improve antiviral immune responses when performed in SIV-infected RMs after more than 2 years of ART[18]. PD-1 blockade was also shown to restore CTL responses in HIV-infected, ART-treated humans *in vivo* in the context of relapsing cancer with prior chemotherapy[11,13]; however, the impact on the HIV reservoir and CTL function has been highly variable[12]. If ICB efficacy is dependent on a critical antigen concentration, restoration of HIV-specific responses may require extensive pretreatment with additional LRAs, as concurrent virus reactivation during ICB was not associated with CTL enhancement.

Dual CTLA-4/PD-1 blockade produced a significant reduction in cell-associated SIV-DNA within LN $CD4^+$ T_{EM}, the $CD4^+$ T-cell subpopulation most activated from combined treatment. Importantly, *in situ* hybridization assays demonstrated a significant reduction in the number of $vRNA^+$ and $vDNA^+$ cells following dual CTLA-4/PD-1 blockade in the LN, including in the BCF. Finally, dual CTLA-4/PD-1 reduced the frequency of LN $CD4^+$ cells harboring intact proviral DNA as determined by IPDA. Of note, PD-1 blockade alone did not impact any measure of viral persistence. We have previously shown that in ART-treated RMs a large fraction of LN $CD4^+PD\text{-}1^+$ T-cells that reside within the BCF that are preferentially enriched for vDNA also express CTLA-4[1]; given their expression of both ICRs, these cells likely represent a preferentially responsive target to dual blockade. Together, these findings suggest a link between viral reactivation and clearance, at least in a subset of infected cells.

Following ART withdrawal, combined blockade did not impact the delay in viral rebound or the set point viral load. In this regard, in the current study ART was initiated at d60 p.i., substantially later than in other NHP studies involving ATI, and therefore with a larger and more disseminated reservoir and development of T-cell exhaustion[32,33]. The inability of the combined blockade to extend the αPD-1 monotherapy-mediated five day delay in viral rebound suggests that αCTLA-4-driven T_{REG} responses and/or some level of reservoir re-seeding caused by viral reactivation may have been sufficient to abrogate the anti-viral synergy between the two treatments[34,35]. Unexpectedly, dual CTLA-4/PD-1 blockade was well-tolerated in NHP, whereas similar regimens were found to be associated with a substantial risk of serious immune-related adverse events in human clinical trials for cancer[36-39]. At present, it is unknown whether CTLA-4 or dual CTLA-4/PD-1 blockade would exhibit acceptable toxicity profiles in ART-treated people living with HIV without co-morbidities. It is plausible that the onset of toxicity could be linked with factors such as the timing of intervention (i.e. the presence and burden of antigen); the duration or interval of therapy; or the extent of T-cell exhaustion (i.e. the frequency and distribution of ICR expression). Our study highlights the need to better understand how tolerability changes in different pre-clinical and clinical settings while balancing the need for immunological efficacy with acceptable profiles of toxicity.

This study represents the first *in vivo* combined ICB in SIV-infected, ART-treated RMs with a high barrier for cure designed to mimic issues pertaining to treatment in people living with HIV; albeit, with a shorter duration of ART than would be expected in humans. We have demonstrated that CTLA-4 blockade in SIV-infected, ART-treated RMs produces robust T-cell proliferation and T_{EM} expansion that synergizes with PD-1 blockade to enhance viral reactivation in PBMCs and plasma; decrease the SIV-DNA content in LN T_{EM}; reduce the

number of vDNA$^+$ and RNA$^+$ cells in the LN BCF; and limit levels of intact provirus in LN. Thus, combined ICB induces latency reversal and a partial reduction of the reactivated reservoir, two critical steps towards eradication of the persistent reservoir of latently HIV-infected cells. Our data highlight the possibility that re-invigoration of antiviral responses through relieving T-cell exhaustion may be dependent on antigen burden. As such, ICB might be more beneficial in antigen-rich phases of HIV infection (such as during ATI or at the time of ART initiation); in subjects that started ART in acute infection, so as to limit the extent of T-cell exhaustion and viral reservoir seeding; or in combination with enhanced killing strategies, such as therapeutic vaccinations[40] or co-administration of neutralizing antibodies[28]. The current study indicates that ICB, even when targeting both PD-1 and CTLA-4, is unlikely to induce HIV remission if performed in the context of sustained aviremia and in the absence of additional interventions.

Methods

Animals, SIV-infection, and antiretroviral therapy

34 male Indian rhesus macaques (RMs; *Macaca mulatto*), all housed at the Yerkes National Primate Research Center (YNPRC) at Atlanta, GA, were included in this study. All RMs were *Mamu*-B*07$^-$ and *Mamu*-B*17$^-$ with the following being *Mamu*-A*01$^+$: RGi16, RKt16, RVr16, RHn16, RPo16, and RZw15. RMs were screened for pathogens and housed as previously described[1].

All RMs were infected intravenously (i.v.) with 300 TCID50 SIVmac$_{239}$ (Fig. 1a). 60 days post-infection (p.i.), all RMs initiated a daily antiretroviral therapy (ART) regimen consisting of dolutegravir (DTG; 2.5 mg/kg/d, subcutaneous; s.c.), tenofovir disoproxil fumarate (TDF; 5.1 mg/kg/d, s.c.), and emtricitabine (FTC; 40 mg/kg/d, s.c.)[41] that was maintained for up to 13.5 months (Extended Data Fig. 1; Extended Data Fig. 2a). RMs were then stratified into treatment groups based on their projected time of virologic suppression under ART, *Mamu*-A*01 status, and presence of anti-drug antibodies (ADAs) during chronic infection (d52 p.i.; Supplementary Fig. 1; Supplementary Table 1). After a minimum of three discontinuous months of undetectable plasma viral loads (181.4 ± 4.9 days; limit of detection ≤60 copies/mL) animals were administered immune checkpoint blockade (ICB) monoclonal antibodies (mAb) once per week over 4 weeks. After a two-week washout period, RMs underwent an ART analytic treatment interruption (ATI) and were followed for up to 7 months with a subsequent necropsy. RFf16 was euthanized at d25 p.i. due to rapid progression to AIDS-defining endpoints, specifically attributable to weight loss.

Study Approval

All animal experimentation was conducted under anesthesia with follow up pain management following guidelines set forth by the Animal Welfare Act and by the NIH's Guide for the Care and Use of Laboratory Animals, 8th edition. All studies were conducted in accordance with institutional regulations including GSK's Policy on the Care, Welfare, and Treatment of Laboratory Animals, and were reviewed and approved by Emory's Institutional Animal Care and Use Committee (IACUC; permit numbers 3000065, 2003297, 2003470, and PROTO201700665). Animal care facilities at YNPRC are accredited by the

U.S. Department of Agriculture (USDA) and the Association for Assessment and Accreditation of Laboratory Animal Care (AAALAC) International.

Immune checkpoint blockade

Immune checkpoint receptor (ICR) blocking monoclonal antibodies (mAb) were developed, formulated, and produced by GlaxoSmithKline and provided via Qura Therapeutics. The described therapeutics are intellectual property of GlaxoSmithKline and are not commercially available. VHDUM, the control, is a fully-human IgG1 mAbdAb with the Fc region disabled by the LAGA mutations: L235A and G237A. The mAb portion has the sequence of palivizumab (anti-respiratory syncytial virus, MedImmune) and is linked by a fibronectin linker to an irrelevant domain antibody that has no known specificity. The IgG4 anti-PD-1 mAb (αPD-1) is a biosimilar formulation of nivolumab (Bristol-Myers Squibb) with a human variable region and a rhesus constant region. The IgG1 anti-CTLA-4 mAb (αCTLA-4) is a fully-human, biosimilar formulation of ipilimumab (Bristol-Myers Squibb) that retains Fcγ binding activity. The IgG1 bispecific αCTLA-4/PD-1 mAbdAb (BsAb) has a human variable and rhesus constant region with a LAGA mutation-disabled Fc receptor, and was constructed with a flexible fibronectin linker connecting the C-terminus of the mAb heavy chain to a PD-1 domain antibody (dAb)[42]. The antagonistic anti-PD-1 dAb was identified through phage display, and bound PD-1-expressing cells with an EC50 of 2 nm; thereby efficiently blocking interactions with PDL-1/PDL-2[43]. The BsAb CTLA-4 is biosimilar to ipilimumab and the PD-1 is a proprietary formulation of GlaxoSmithKline (Extended Data Fig. 2b). Optimal dosing concentrations and intervals were determined in a pharmacokinetics (PK) and pharmacodynamics (PD) pilot study in drug-naïve, un-infected RMs conducted by Convance Research Products on behalf of GlaxoSmithKline (data not shown).

Pre-filtered, endotoxin-free compounds were provided in sterile, glass dosing vials that were stored long-term at −80°C. Agents were administered under anesthetic sedation as an i.v. bolus push over approximately 15 mins without pre-treatment prophylaxis. Doses administered were as follows: control, 30 mg/kg (n=6); αCTLA-4, 5 mg/kg (n=6); αPD-1, 5mg/kg (n=6); αCTLA-4 plus αPD-1 (combined blockade), 5 mg/kg each (n=7); and BsAb, 5 mg/kg (n=8). Diphenhydramine (1-2 mg/kg, i.v.) and dexamethasone (0.3 mg/kg, i.v.) were available in the event of a suspected adverse event, such as anaphylaxis or respiratory distress. Endpoint criteria included the onset of adverse events that required steroids to control.

Sample collection and processing

Collections of peripheral blood (PB) and lymph node (LN) biopsies were conducted longitudinally and at necropsy (Fig. 1a) as previously described[1] with the following exception: during ICB infusions, blood was drawn prior to and 5 mins afterwards for pharmacokinetic assays.

Flow cytometric analysis

Eighteen-parameter flow cytometric analysis was performed on peripheral blood mononuclear cells (PBMCs) and mononuclear cells derived from LN biopsies. Samples

were stained utilizing standard procedures with anti-human mAbs that we, and others, have shown to be cross-reactive in RMs[1,44] and those clones verified as RM reactive (NHP Reagent Resource). The following antibodies were used at predetermined optimal concentrations for the longitudinal staining panel: anti-T-bet-PE/Dazzle-594 (clone 4B10; cat# 644828), anti-FoxP3-APC (clone 150D; cat# 320014), anti-CD4-APC-Cy7 (clone OKT4; cat# 317418), anti-CD95-BV605 (clone DX2; cat# 305628), anti-HLA-DR-BV650 (clone L243; cat# 307650), anti-CD25-BV711 (clone BC96; cat# 302636), anti-CD20-PerCp/Cy5.5 (clone 2H7; cat# 302326), and anti-PD-1-BV785 (clone EH12.2H7; cat# 329930) all from Biolegend; anti-CXCR5-PE (clone MU5UBEE; cat# 12-9185-42) and anti-CD127-PE-Cy5 (clone eBioRDR5; cat# 15-1278-42) both from eBioscience; anti-CCR7-PE-Cy7 (clone 3D12; cat# 557648), anti-Ki-67-Alexa700 (clone B56; cat# 561277), anti-CTLA-4-BV421 (clone BNI3; cat# 562743), anti-CD3-BUV395 (clone SP34-2; cat# 564117), anti-CD8-BUV496 (clone RPA-T8; cat# 564804), and anti-CD28-BUV737 (clone CD28.2; cat# 564438) all from BD Biosciences; anti-LAG-3-FITC (clone 17B4; cat# NBP1-97665) from Novus Biologicals; and Aqua Live/Dead amine dye-AmCyan from Invitrogen (cat# L34966). The following antibodies were used for phenotyping cryo-preserved LN: anti-CD200-PE (clone OX104; cat# 329206), anti-HLA-DR-PE-Cy5 (clone L243; cat# 307608), anti-CD4-APC-Cy7 (clone OKT4; cat# 317418), anti-CD25-BV711 (clone BC96; cat# 302636), anti-CD101-PerCP/Cy5.5 (clone BB27; cat# 331016), anti-CD95-BV605 (clone DX2; cat# 305628), and anti-CD69-BV785 (clone FN50; cat# 310932) all from Biolegend; anti-CD38-FITC (clone AT-1; cat# 10415) from STEMCELL Technologies; anti-CCR7-PE-Cy7 (clone 3D12; cat# 557648), anti-Ki-67-Alexa700 (clone B56; cat# 561277), anti-CTLA-4-BV421 (clone BNI3; cat#562743), anti-CXCR3-BV650 (clone 1C6/CXCR3), anti-CD3-BUV395 (clone SP34-2; cat# 564117), anti-CD8-BUV496 (clone RPA-T8; cat# 564804), and anti-CD28-BUV737 (clone CD28.2; cat# 564438) all from BD Biosciences; anti-PD-1-Alexa647 (clone 913429; cat# MAB10861; 1:50 dilution) from Novus Biologicals; and anti-Granzyme B-PE-Texas Red (clone GB11; cat# GRB17) and Aqua Live/Dead amine dye-AmCyan from Invitrogen (cat# L34966). The following panel of antibodies was utilized for measuring cytolytic and SIV-specific responses in cryo-preserved cells: anti-CD3-BUV395 (clone SP34-2; cat# 564117), anti-CD8-BUV496 (clone RPA-T8; cat# 564804), anti-Ki-67-AL700 (clone B56; cat# 561277), anti-CD95-PE-Cy5 (clone DX2; cat# 559773), anti-CCR7-BV480 (clone 3D12; cat# 566099), anti-GranzymeB-BV421 (clone GB11; cat# 563389), and anti-CD28-BUV737 (clone CD28.2; cat# 612815) all from BD Biosciences; anti-HLA-DR-BV750 (clone L243; cat# 307672), anti-CD4-BV570 (clone OKT4; cat# 317445), anti-PD-1-BV786 (clone EH12.2H7; cat# 329930), and anti-CTLA-4-PE (clone BNI3; cat# 369604) all from Biolegend; anti-Gag-APC (clone CM9; 4.2 μg/test) from the NIH Tetramer Facility at Emory University;[45] anti-CD38-APC (clone AT-1; cat# 60131FI) from STEMCELL Technologies; and anti-EOMES-PE-eFluor610 (clone WD1928; cat# 611-4877-42) and LIVE/DEAD Fixable Near-IR Dead Cell Stain from Thermo Fisher Scientific (cat# L34976). All mAbs were used at the manufacturer's recommended test volume per 10^6 mononuclear cells (1:100 dilution) unless otherwise noted.

Purified anti-PD-1 (clone 913429; cat# MAB10861; Novus Biologicals) was labeled using an Alexa Fluor 647 Antibody Labeling Kit (Invitrogen) using the manufacture's guidelines.

To detect intracellular expression of FoxP3, mononuclear cells were fixed and permeabilized with FoxP3/Transcription Factor Staining Buffer Kit Fix/Perm (Tonbo), and subsequently stained intracellularly; otherwise a BD Cytofix/Cytoperm kit (BD Biosciences) was employed. To determine the *ex vivo* expression of CTLA-4$^+$ in CD4$^+$ and CD8$^+$ T-cells, staining was performed intracellularly in unstimulated T-cells[1]. Flow cytometry acquisition was performed on a minimum of 120,000 live CD3$^+$ T-cells for LN and PBMC. Data acquisition was performed on an LSRFortessa or FACSymphony (BD Biosciences) driven by FACS DiVa software and analyzed using FlowJo software (version 9.9.6; TreeStar).

Flow cytometry cell sorting

Cryo-preserved, unstimulated mononuclear cells derived from LN biopsies were stained with the following combination of RM-reactive, anti-human mAbs (NHP Reagent Resource)[1,44]: anti-CD200-PE (clone OX104; cat# 329206), anti-CD25-Alexa700 (clone BC96; cat# 302622), and anti-CD4-BV650 (clone OKT4; cat# 317436) all from Biolegend; anti-CD28-PE-CF594 (clone CD28.2; cat# 562296), anti-CCR7-PE-Cy7 (clone 3D12; cat# 557648), anti-CD3-APC-Cy7 (clone SP34-2; cat# 557757), and anti-CD95-BV421 (clone DX2; cat# 562648) all from BD Biosciences; anti-CD8-FITC (clone 3B5; cat# MHCD0801) and Aqua Live/Dead amine dye-AmCyan from Invitrogen (cat# L34966); anti-CD127-PE-Cy5 (clone eBioRDR5; cat# 15-1278-42) from eBioscience; and anti-PD-1-Alexa647 (clone 913429; cat# MAB10861; 1:50 dilution) from Novus Biologicals. All mAbs were used at the manufacturer's recommended test volume (1:100 dilution) scaled per 10^7 mononuclear cells unless otherwise noted. Purified anti-PD-1 was labeled using an Alexa Fluor 647 Antibody Labeling Kit (Invitrogen) using the manufacture's guidelines. The following memory subsets of CD4$^+$ T-cells were sorted on a FACS AriaII (BD Biosciences): T_{FH} (T follicular helper), T regulatory (T_{REG}), effector-memory (T_{EM}), and central-memory (T_{CM}). For phenotypic discrimination, T_{FH} were defined as PD-1^{hi}CD200^{hi}; whereas, T_{REG} (CD25$^+$CD127$^-$) were pre-gated as PD-1^{lo}CD200^{lo} to avoid the inclusion of CD25$^+$ T_{FH} T-cells and T follicular regulator (T_{FREG}) cells[46]. Within the CD25$^-$PD-1^{lo}CD200^{lo} population the T_{EM} and T_{CM} were sorted based on their CCR7 expression. Sorted CD4$^+$ T-cell subsets were on average >96% pure as determined by post-sorting flow cytometry analysis. See Fig. 5a for a representative gating strategy.

Determination of viral load RNA

The number of SIVmac$_{239}$ RNA copies per mL of plasma was quantified, as previously described, by quantitative reverse transcription polymerase chain reaction (RT-qPCR)[47] or by PCR[48] with a limit of detection of 15 copies/mL and 60 copies/mL, respectively; therefore, the higher limit of detection was utilized for all data sets.

Quantitation of cell-associated SIV-DNA and -RNA

Analyses were performed on FACS-sorted memory CD4$^+$ T cell-subsets from LN biopsies and on bulk snap frozen PBMCs. SIV-DNA and -RNA was extracted using an AllPrep DNA/RNA Mini Kit (Qiagen). SIV-DNA and -RNA in tissue was assessed using hybrid real-time/digital PCR and RT-qPCR assays in 12 replicate reactions with single copy clinical sensitivity as previously described[49]. Viral copy numbers were reported normalized based on

CCR5 DNA copy numbers. Assays for which there were fewer than 10 positive amplifications per replicates were calculated using Poisson methods.

Chromogenic SIV-RNA and –DNA in situ hybridization and image analysis

RNAscope was performed on formaldehyde-fixed, paraffin-embedded (FFPE) tissue sections (5 mm) according to our previously published protocol[27] with the following minor modifications: heat-induced epitope retrieval was performed by boiling slides in 1x target retrieval (322000; ACD) for 30 min, followed by incubation at 40°C with a 1:10 dilution of protease III (322337; ACD) in 1x PBS for 20 min. Slides were incubated with the target probe $SIVmac_{239}$ (312811; ACD) for 2 hours at 40°C. Amplification was performed with RNAscope 2.5 HD Detection kits (322360; ACD) according to manufacturer's instructions with 0.5X wash buffer (310091; ACD) used between steps. The resulting signal was detected with Warp Red chromogen (WR806M; Biocare Medical). Slides were counterstained with CAT hematoxylin (CATHE-GL; Biocare Medical), mounted with Clearmount (17885-15; EMS) until dry, cover slipped using Permount (SP15-100; Fisher Scientific); and scanned at 40x magnification on an Aperio AT2 (Leica Biosystems). DNAscope was performed on FFPE tissue sections as above except that a 1:5 dilution of protease III and an in-house 3% H_2O_2 in PBS solution were used, slides were incubated with the target probe $SIVmac_{239}$ sense (314071; ACD) for 4 hours at 40°C, and the wash steps after amplification steps 5 and 6 were performed using 1X Tris-buffered saline with 0.05% Tween-20 (TBS-T).

Quantitative image analysis of RNAscope whole tissue images was performed to determine the total number of SIV $vRNA^+$ cells/10^5 total cells using the CytoNuclear module (v1.6) within Halo software (v2.3.2089.27; Indica Labs). Specific regions of the lymph node (B-cell follicle, T-cell zone and medullary cord) were manually highlighted in Halo based on CD4/CD20 staining of subjacent slides. Using the Stain 1 Min OD slider in the CytoNuclear module on concomitantly assayed, early chronic infection SIV^+ control slides, we set the vRNA minimum signal size to exclude detection of the smaller single vRNA and/or vDNA molecules. DNAscope images were analyzed for the total number of $vDNA^+$ cells/10^5 total cells using the ISH module (v3.0.2; for quantifying the number of $vDNA^+$ cells) and the CytoNuclear module (v1.6; for quantifying the number of total cells) within Halo. We set the vDNA minimum and maximum signal spot size by adjusting the Probe 1 spot size setting in the ISH 3.0.2 module on SIV^+ control slides to capture only cells with one, and occasionally more than one, clear punctate dots within their nuclei. In all quantifications, manual curation was performed on each sample to correct for false positives/false negatives. Analyses were performed blinded for ICB therapy.

Fluorescence multiplex SIV-RNA and -DNA in situ hybridization with CD3 and myeloid cell staining and image analysis

DNAscope and RNAscope was performed sequentially as described above, with the following modifications: for DNAscope, slides were kept wet following paraffin removal and antigen retrieval prior to the addition of the $SIVmac_{239}$ sense (314071; ACD) probe for 14 hours at 40°C. Amplification was performed with the RNAscope 2.5 HD Detection kit - Brown (322310; ACD) and the signal was developed with tyramide-conjugated Alexa Fluor 647 (B40958; Invitrogen). Slides were placed for 10 minutes in 1x target retrieval (322000;

ACD) at 95°C, cooled, and probed for 2 hours with SIVmac$_{239}$ (312811; ACD). Following amplification as above, the signal was developed with tyramide-conjugated Alexa Fluor 568 (B40956; Invitrogen). Slides were then incubated overnight with antibodies against the myeloid markers CD68 (CM033C; Biocare) and CD163 (MA5-11458; Invitrogen) at 1:400 each, and the T-cell marker CD3 (RM-9107-S; Thermo Scientific) at 1:200, and detected with donkey anti-mouse Alexa Fluor 488 (A21202; Invitrogen) and donkey anti-rabbit DyeLight 755 (SA5-10043; Invitrogen) at 1:500 for 1 hour, respectively.

To quantify the number of SIV vDNA$^+$ lymphocytes or myeloid cells on stained tissues, whole slide high-resolution fluorescent scans were performed at 20X using the Zeiss Axioscan Z.1 slide scanner. DAPI, Alexa Fluor 488, Cy5 (For Alexa Fluor 647) and Cy7 (For Alexa Fluor 750) channels were used to acquire images. The exposure time for image acquisition was between 4 and 150 ms. Multi-spectral images were analyzed using the HALO 2.3 platform (Indica Labs) using the following analysis methods: For SIV vDNA, cells with clear punctate dots were quantified using the module FISH v1.1. using a similar thresholding method as in the analysis of the chromogenic staining. Putative positive signals were further selected by fine filtering based on signal area and average intensity. For quantification of SIV vRNA$^+$ cells, the same FISH v1.1 module was also used with a minimum signal size set to exclude cells with single vRNA/vDNA signals. Manual curation was performed on each sample to correct for false positives/false negatives. High resolution representative images were taken using the Keyence BZ-X710 fluorescence microscope with the 20X objective using the Z-stack and Full Focus functions. The exposure time for image acquisition was between 2 ms and 10 s.

Quantification of anti-drug antibodies in plasma

Plasma samples collected before and after antibody infusion were thawed, mixed with assay diluent (Casein in PBS, Thermo Fisher Scientific), and added to the assay plate along with two concentrations (low and high) of the positive control (JDC-10, Southern Biotech) and a negative control (pool of normal RM plasma). Each antibody was biotinylated and sulfo-tagged with a 1:1 mixture of biotin-Ab and sulpho-tag-Ab at 1 μg/ml in Casein and added to the assay plate. The assay plate was sealed and placed on a shaker for greater than 2 hours at room temperature to allow complex formation. During the incubation, blocking buffer (Smartblock, Candor Biosciences) was added to a Meso Scale Discovery (MSD) standard streptavidin plate for 2 hours at room temperature with shaking. Blocking solution was removed from the MSD-SA plate and 50 μl of sample from the assay plate was added in duplicate to MSD-SA blocked plates. Plates were sealed; incubated in the dark for 1 hour with continuous shaking; washed 3 times with 300 μl PBS with 0.1% Tween 20; and MSD read buffer was added. Plates were read on an MSD Imager and the levels of anti-drug antibodies were quantified by electrochemiluminescence (ECL).

Determination of pharmacokinetics of monoclonal antibodies in plasma

The respective antigen (CTLA-4 or PD-1 protein) was diluted into PBS and coated onto each well of a microtiter plate for at least 12 hours at 4°C. Plates were washed 5-fold with 25mM Tris, 150 mM NaCl, 0.1% Tween 20, pH 7.5 (wash buffer). 150 μl of blocking assay buffer (Superblock TBS-T20, Thermo Fisher Scientific) was added, and the plates were

sealed and incubated for at least 1 hour with constant shaking. Plasma samples collected pre- and 5 mins post-infusion were serially diluted 50-fold into assay buffer. Samples needing further dilution were diluted into assay buffer containing 2% cynomolgus macaque serum. After washing, sample was added to each well of the microtiter plate as appropriate: test sample, blank, calibration standard, or quality controls (i.e antibody diluted into plasma from healthy RMs, Bioreclamation). Plates were sealed and incubated with constant shaking for 2 hours at 37°C. Plates were then washed, detection solution added (ruthenium-labelled mouse anti-human IgG Fc JDC-10 from Southern Biotech or ruthenium-labelled PD-1 from GSK), and plates were incubated with constant shaking for 1 hour at 37°C. Plates were once again washed, read buffer T (Meso Scale Discovery) was added to each well, and plates were read within 5 mins on an MSD Sector S600.

Enzyme-linked immune absorbent spot (ELISpot) for the quantification of Interferon gamma response upon SIV-Gag and -Env stimulation

Cryo-preserved PBMCs and lymph node-derived mononuclear cells were thawed, rested, and triplicate plated at of $4x10^5$ cells per well. Cells were either unstimulated (DMSO) or stimulated with $SIVmac_{239}$ overlapping Gag/Env peptides (NIH AIDS Reagent Program) at a concentration of 1 μg/ml, or with Concavalin A (Sigma) at 2.5 μg/ml. Plates were incubated for 24 hours at 37°C and the number of cells secreting IFN-γ were evaluated using the Monkey IFN-γ $ELISpot^{PLUS}$ kit (MABTECH) per manufacturer's instructions. The number of spot-forming units (SFU) per well were enumerated on an ELISpot plate reader and expressed as SFU per million cells. The IFN-γ response is shown as an average of triplicate reactions with the DMSO background subtracted out.

Determination of intracellular cytokine induction following SIV-Gag and -Env peptide stimulation

Cryo-preserved PBMCs were thawed, rested, and resuspended in RPMI 1640 (Invitrogen) supplemented with 10% Fetal Bovine Serum (Seradigm) in the presence of Golgi transport inhibitors, anti-CD107a-APC (clone H4A3; cat# 328620) from Biolegend, anti-CD49D (clone 9F10; cat# 304302) from BD Biosciences, and anti-CD28-PE-Cy7 (clone CD28.2; cat# 25-0289-42) from eBiociences. PBMCs were either left unstimulated (DMSO) or stimulated for 6 hours at 37°C with either $SIVmac_{239}$ overlapping Gag/Env peptides (NIH AIDS Reagent Program) at a concentration of 1 μg/ml or staphylococcal enterotoxin A & B (SEB/A- List Biologicals) at 250 ng/ml. After stimulation, cells were washed and stained for cell surface antigens with the following combination of mAbs: anti-CD3 Alexa-700 (clone SP34-2; cat# 557917), anti-CD95 BB515 (clone DX2; cat# 564596), and anti-CD4 BV711 (clone L200; cat# 563913) all from BD Bioscience; anti-CD8 PerCP-Cy5.5 (clone RPA-T8/SK1; cat# 344710) and anti-PD-1 BV421 (clone EH12; cat# 329920) both from Biolegend; and the Live/Dead Amine Aqua Dye from Life Technologies (cat# L34966). To detect intracellular expression of cytokines, mononuclear cells were fixed and permeabilized with a Cytofix/Cytoperm kit (BD Biosciences) and stained as follows: anti-TNF-α BV650 (clone Mab11; cat# 563418) and anti-IL-2 PE (clone MQ1-17H12; cat# 500307) both from Biolegend, and anti-IFN-γ PE-CF594 (clone B27; cat# 562392) from BD Biosciences. All mAbs were used at the manufacturer's recommended test volume (1:100 dilution). The frequency of SIV-specific memory $CD4^+$ and $CD8^+$ T-cells producing single or multiple

cytokines was determined after background subtraction. Cytokine co-expression data was processed using Pestle and SPICE version 6 (NIAID)[50].

Intact Proviral DNA Assay

From LN biopsy-derived, cryo-preserved mononuclear cells, $CD4^+$ cells were isolated using non-human primate CD4 Microbeads (Miltenyi Biotec) and genomic DNA was extracted with a QIAamp DNA Mini Kit (QIAGEN). The intact proviral DNA assay (IPDA) was performed as described[26,51], with modifications. As the SIV IPDA was originally designed for $SIVmac_{251}$, we adjusted the reverse primer for *env* to match the $SIVmac_{239}$ consensus sequence: 5'-GTTGTTATTGATTTTGTCAATCCC-3' (NCBI GenBank, accession number M33262). 8 replicate wells of 500 ng DNA each were combined with 2X ddPCR Supermix for Probes (no dUTP, Bio-Rad) and primer/probe sets for regions in *pol* and *env* that favors amplification of intact proviral genomes. In addition, 8 replicate wells of 500 ng DNA each were combined with ddPCR Supermix and primer/probe sets for 2-LTR circles and intact *env*, as described. Droplets were generated on the Automated Droplet Generator (Bio-Rad), and subsequently underwent thermocycling for 10 minutes at 95°C for 45 cycles (30 seconds at 94°C and 60 seconds at 57°C per cycle) and 10 minutes at 98°C. Droplets were read on the QX100 Droplet Reader (Bio-Rad). Replicate wells were merged and analyzed in the QuantaSoft Analysis Pro Software. As described by Bender et al., a correction for shearing was not applied given low and similar shearing rates across samples, and the frequency of 2-LTR^+env^+ circles was subtracted from the frequency of intact (pol^+env^+) proviruses[26,52]. Samples with a DNA shearing index of greater than 25 were excluded from analyses (RWs16 at day −29 p.t.; Extended Data Fig. 7c), and limited cell numbers prevented analyses in 3 controls and 1 BsAb-treated RMs.

Genome Sequencing

Single-genome sequencing of gp160 *env* sequences were generated as previously described[53]. Briefly, plasma was centrifuged; vRNA was extracted using the EZ1 Virus Mini Kit v2.0 (Qiagen); and cDNA was synthesized using reverse primer SHIV.Env.R1 (5'-TACCCCTACCAAGTCATCA -3'), and used for limiting-dilution nested PCR. Amplicons of correct size were sequenced using the MiSeq platform (Illumina). Raw reads were aligned to $SIVmac_{239}$ reference using Geneious version R11. Sequences with evidence of mixed templates were excluded from further analysis. Maximum-likelihood phylogenetic trees were generated using the HKY85 substitution model and a transition/transversion ratio of four in PhyML Version 3.0 (ATGC Bioinformatics) and visualized in FigTree[54]. Lineages were deemed distinct if they differed at 3 or more nucleotide positions over *env*. Sequences are available in GenBank (accession numbers MN856887 – MN857133).

Sequencing was performed on plasma from chronic infection prior to ART initiation (d52 p.i.; n=2); during on-ART, ICB-mediated viral reactivation (n=8); and immediately following ATI (n=8). A total of 248 sequences (median 13 per sample) were obtained. During chronic infection (d52 p.i.) RTj16 and RZl16 had a maximum divergence from the $SIVmac_{239}$ inoculum strain of 6 and 8 nucleotides (0.2-0.3%) and a maximum diversity of 9 and 13 nucleotides (0.3-0.5%), respectively. This degree of diversity enables enumeration of

virus lineages, which provides a minimum estimate of the number of infected cells contributing to plasma viremia during ICB reactivation and rebound post-ATI.

CellTrace Proliferation Tracking

Cryo-preserved PBMCs were thawed, rested overnight, and washed with PBS. Cells were labeled with 5 μM CellTrace Violet (cat# C34557; Thermo Fisher Scientific) in PBS at 37°C in a dark water bath and quenched for 5 min over ice in the presence of 10% FBS (Gemini Bio-products). CellTrace-labeled PBMCs were washed and resuspended ($2.5x10^6$ cells/mL) in RPMI 1640 medium supplemented with 10% heat-inactivated FBS, 100 U/mL penicillin, 100 μg/mL streptomycin, 20 U/mL recombinant human IL-2 (Gemini Bio-products), 5 μg/mL anti-CD28-BUV737 (clone CD28.2; cat# 612815; BD Biosciences), and 5 μg/mL anti-CD2 (clone RPA-2.10; cat# 300202; Biolegend). Cells were plated on anti-CD3 (clone SP34-2; cat# 551916; BD Biosciences; 1 μg/well) coated 96 well polystyrene plates and incubated at 37°C with 5% CO_2 over water. Stimulated cells were with fed with fresh media supplemented with 20 U/mL IL-2 (final concentration) at d3 and were harvested at d6. After stimulation, cells were washed and stained with the following combination of monoclonal antibodies: anti-CD3-BUV395 (clone SP34-2; cat# 564117), anti-CD8-BUV496 (clone RPA-T8; cat# 612942), anti-Ki-67-AL700 (clone B56; cat# 561277), anti-CD95-PE-Cy5 (clone DX2; cat# 559773), anti-CCR7-PE-Cy7 (clone 3D12; cat# 557648), and anti-CD28-BUV737 (clone CD28.2; cat# 612815) all from BD Biosciences; anti-CD4-PerCP-Cy5.5 (clone OKT4; cat# 317428), anti-PD-1-BV786 (clone EH12.2H7; cat# 329930), and anti-CTLA-4-PE (clone BNI3; cat# 369604) all from Biolegend; and LIVE/DEAD Fixable Near-IR Dead Cell Stain (cat# L34976) from Thermo Fisher Scientific. All mAbs were used at the manufacturer's recommended test volume (1:100 dilution) per 10^6 cells unless otherwise noted. Samples were collected on a FACSymphony (BD Biosciences) and proliferation curves were analyzed in FlowJo (version 9.9.6; TreeStar).

Statistical Analysis

All statistical tests were two-sided and p-values ≤0.05 (95% confidence interval) were considered statistically significant for each of the specific statistical comparisons (*, $p<0.05$; **, $p<0.01$; ***, $p<0.001$; ****, $p<0.0001$). Data showing continuous outcomes are represented as mean ± SEM. All measurements were taken from distinct samples with the exception of IFN-γ ELISpot (3 replicates); IPDA (8 replicates); and cell-associated SIV-DNA/RNA (12 replicates). Gaussian distribution conformity was tested using the D'Agostino-Pearson omnibus normality test. Correlations were performed using a Pearson correlation coefficient. A two-way ANOVA, or a mixed-effects model if data points were absent, was utilized to calculate significance for longitudinal, treatment-stratified data sets. All two-way ANOVAs employed row stacking for repeated measurements; multiple comparisons with Dunnett's or Bonferroni's correction for simple effects within rows relative to control or within columns relative to treatment baseline; and p-values are reported as a multiplicity between the directions of comparison. Cross-sectional comparisons of parameters at a solitary time point were calculated using either a Mann-Whitney U tests; Wilcoxon Rank-Sum test; or a Kruskal-Wallis test with Dunn's correction for multiple comparisons. Pie chart distributions were analyzed using a Permutation test (10,000 iterations) in SPICE version 6. SIV-DNA and -RNA measurements were excluded for

samples if <10,000 cells were sorted and values fell outside the assay limit of detection. IPDA data were excluded if they had a DNA shearing index of greater than 25. Analyses were conducted using GraphPad Prism 8.1.2.

Extended Data

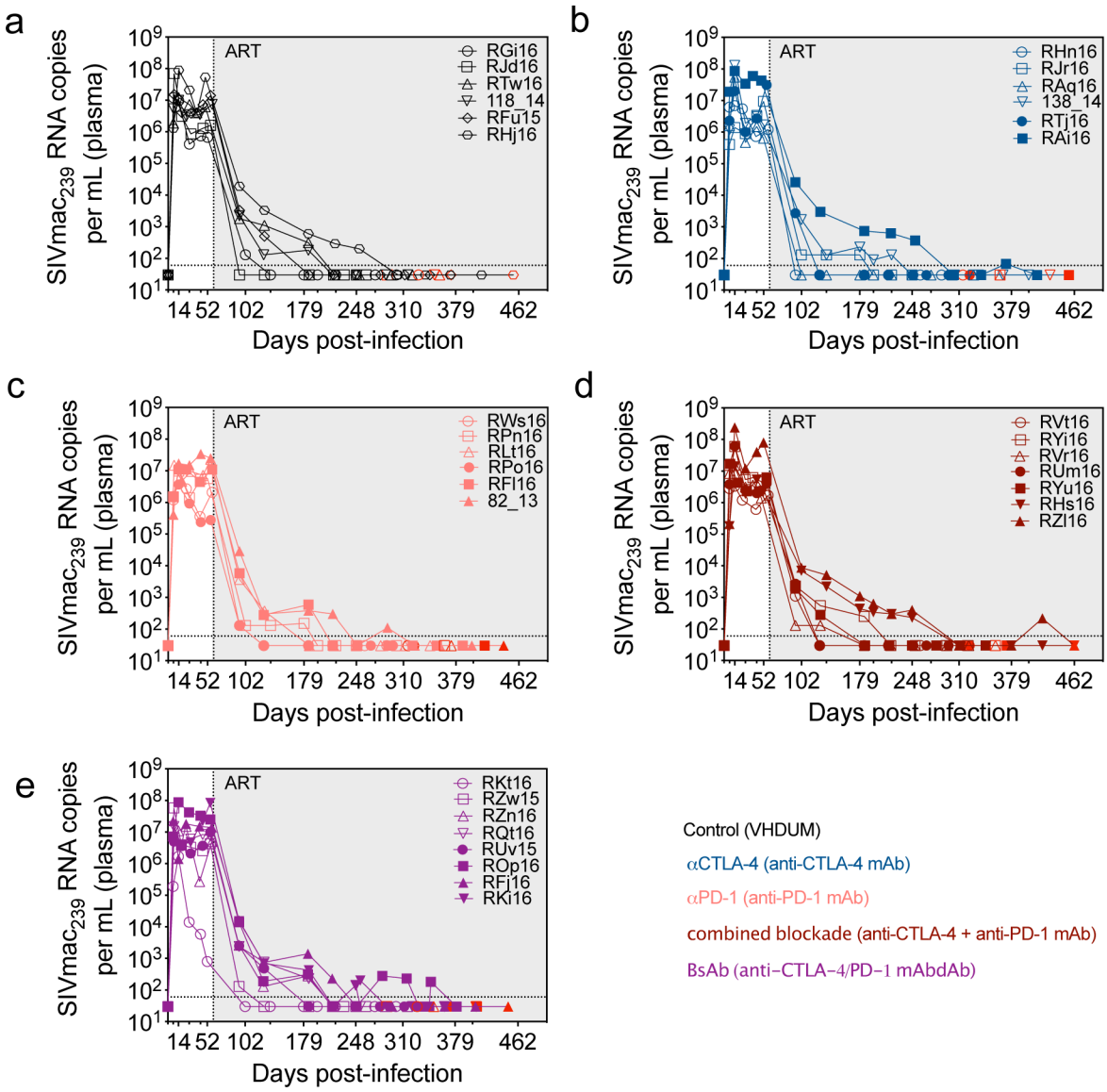

Extended Data Figure 1. Plasma viral loads during acute SIV infection and subsequent decay during ART.

Viral loads ($SIVmac_{239}$ RNA copies/mL) were quantified in plasma utilizing RT-qPCR and represented on a logarithmic scale. The terminal measurement (indicated in light red) for each animal indicates the start of ICB therapy (d0 p.t.). Initiation of ICB therapy was dependent on duration of undetectable viremia in plasma. Data sets are grouped based on ICB treatment as follows: (**a**) VHDUM (control; n=6), black; (**b**) anti-CTLA-4 mAb (αCTLA-4; n=6), blue; (**c**) anti-PD-1 mAb (αPD-1; n=6), pink; (**d**) anti-CTLA-4 plus anti-

PD-1 mAb (combined blockade; n=7), red; and (**e**) anti-CTLA-4/PD-1 mAbdAb (BsAb; n=8), purple. Individual RMs are indicated by shape with closed data points indicating viral reactivation in plasma during subsequent ICB. The vertical dashed line indicates ART initiation (d60 p.i.) and the shaded gray area represents ongoing ART administration. The horizontal dashed line indicates the assay's limit of detection (≤60 copies/mL) with undetectable events represented as 30 copies/mL.

a

Animal ID	Sex	*Mamu**A01 genotype	Age (months)[a] Infection	Age (months)[a] ICB	#CD4[b] pre-ART	Viral load (copies/mL)[c] acute	Viral load (copies/mL)[c] pre-ART	UD Viral Load[d] (days)	ICB Treatment	Annotated Symbol
RGi16	M	+	31	41	748	9.7E+06	6.7E+05	195	control	○
RJd16	M	-	42	51	1474	3.1E+06	1.6E+06	195	control	□
RTw16	M	-	27	39	1753	1.2E+07	6.1E+06	138	control	△
118_14	M	-	27	38	1809	9.9E+06	7.4E+06	134	control	▽
RFu15	M	-	44	56	690	4.1E+06	1.4E+07	187	control	◇
RHj16	M	-	30	45	1292	8.9E+07	5.3E+07	152	control	⬡
RHn16	M	+	30	40	1824	6.9E+06	1.2E+06	221	αCTLA-4	○
RTj16	M	-	31	41	1390	2.0E+07	3.1E+07	198	αCTLA-4	●
RJr16	M	-	29	41	1405	1.4E+06	9.5E+06	167	αCTLA-4	□
RAq16	M	-	29	41	1600	5.5E+07	6.4E+05	262	αCTLA-4	△
138_14	M	-	25	39	269	1.3E+08	1.7E+06	182	αCTLA-4	▽
RAi16	M	-	31	46	2946	8.6E+07	4.3E+07	152	αCTLA-4	■
RWs16	M	-	29	39	530	1.2E+07	2.1E+06	190	αPD-1	○
RPo16	M	+	30	41	2099	3.7E+06	2.8E+05	198	αPD-1	●
RPn16	M	-	29	41	826	9.8E+06	5.7E+06	167	αPD-1	□
RLt16	M	-	30	42	988	4.7E+06	2.3E+07	187	αPD-1	△
RFl16	M	-	30	44	1572	1.1E+07	1.1E+07	200	αPD-1	■
82_13	M	-	42	56	N/A	1.7E+07	2.5E+07	193	αPD-1	▲
RVt16	M	-	29	39	779	3.3E+06	1.7E+06	190	combined	○
RUm16	M	-	30	41	2209	6.1E+07	4.1E+06	198	combined	●
RYi16	M	-	31	42	1764	6.0E+07	4.6E+06	138	combined	□
RVr16	M	+	29	41	1161	1.5E+07	1.4E+06	173	combined	△
RYu16	M	-	30	42	1127	4.3E+06	6.3E+06	187	combined	■
RZl16	M	-	30	45	2080	2.4E+08	8.0E+07	152	combined	▲
RHs16	M	-	28	44	555	1.4E+07	2.4E+06	152	combined	▼
RKt16	M	+	28	39	2746	1.7E+06	8.0E+02	227	BsAb	○
RZw15	M	+	43	53	439	3.9E+06	4.3E+06	162	BsAb	□
RZn16	M	-	30	41	525	1.1E+07	5.0E+06	134	BsAb	△
RUv15	M	-	43	56	1416	3.6E+06	9.9E+06	187	BsAb	●
ROp16	M	-	30	43	2571	8.8E+07	2.5E+07	191	BsAb	■
RFj16	M	-	31	45	857	1.4E+06	1.4E+07	200	BsAb	▲
RQt16	M	-	30	43	583	3.8E+06	7.5E+06	189	BsAb	▽
RKi16	M	-	32	46	3267	4.1E+06	8.4E+07	188	BsAb	▼

b

Treatment	abbreviation	Format	Isotype	Fc disabled[e]	Constant region	variable region	Bio-similar equivalent[f]	dose (mg/kg)	route
VHDUM	control	mAbdAb	IgG1	Yes	human	human	Palivizumab	30	i.v.
anti-PD-1	αPD-1	mAb	IgG4	Yes	rhesus	human	Nivolumab	5	i.v.
anti-CTLA-4	αCTLA-4	mAb	IgG1	No	human	human	Ipilimumab	5	i.v.
anti-CTLA-4/PD-1	BsAb	mAbdAb	IgG1	Yes	rhesus	human	Ipilimumab / proprietary	5	i.v.

Extended Data Figure 2. Characteristics macaques and ICB antibodies.

[a]Age in months at SIV infection (d0 p.i.; post-infection) and at ICB (d0 p.t.; post-treatment).

[b]Indicates the number of $CD4^+$ T-cells per μL of PB at chronic infection prior to ART initiation (d52 p.i.) as determined by complete blood counts combined with flow cytometry.

[c]SIV-RNA viral loads per mL of plasma was measured by quantitative RT-qPCR with a limit of detection of ≤60 copies/mL at acute (d14 p.i) and chronic infection (d52 p.i.).
[d]Days of undetectable (UD) viral load prior to ICB treatment were calculated from the first UD observation following ART initiation and does not account for subsequent blips.
[e]Indicates whether Fc gamma receptor has been disabled by a LAGA mutation (L235A and G237A) and is capable of antibody-dependent cellular cytotoxicity (ADCC), antibody-dependent cellular phagocytosis (ADCP), ect.
[f]Indicates the pharmacological generic equivalent of the variable domain and epitope specificity.

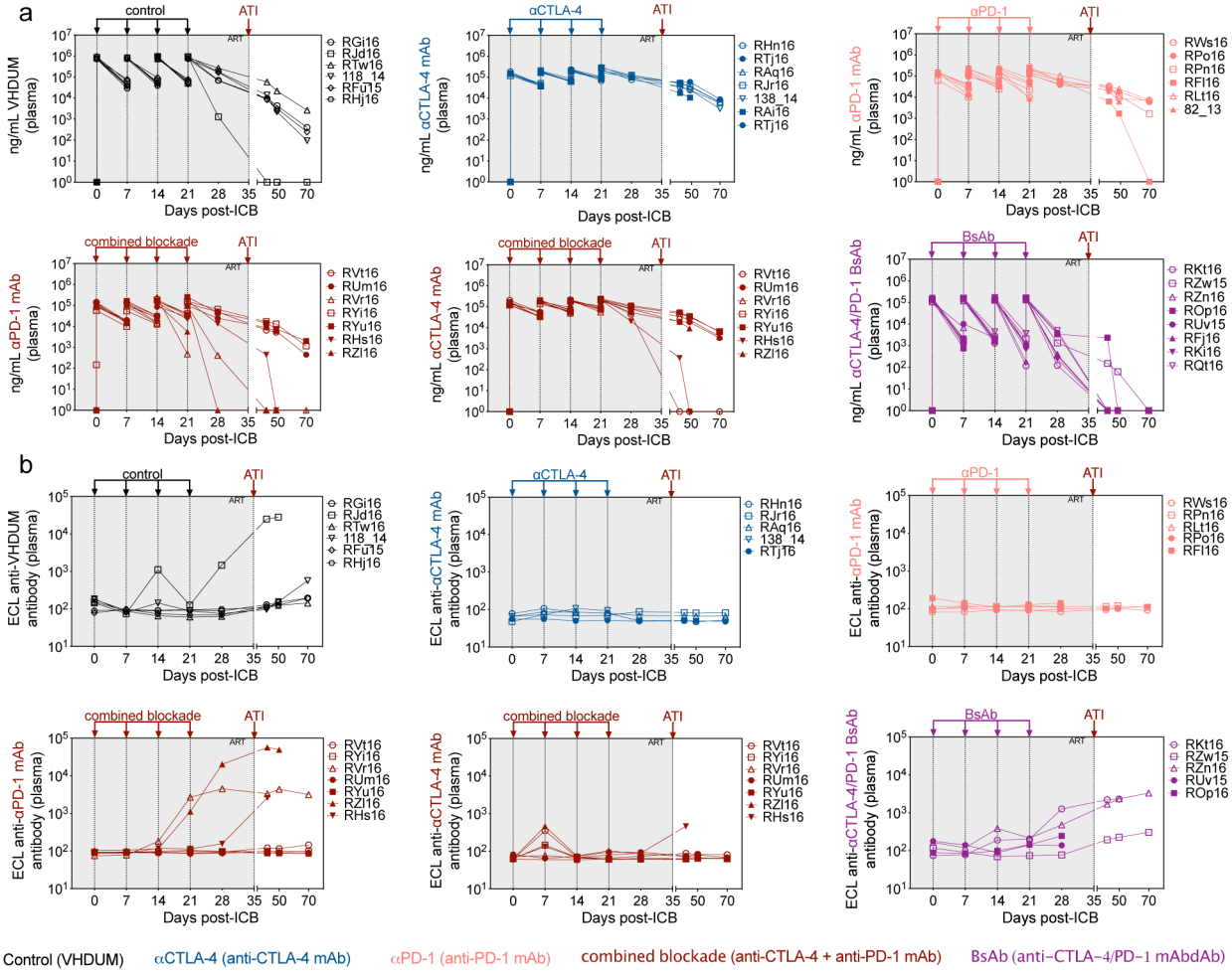

Extended Data Figure 3. Blockade pharmacokinetics and emergence of anti-drug antibodies.
(**a**) Plasma concentrations (ng/mL) of Co-IR blocking monoclonal antibodies (mAb) were quantified with an antibody capture assay; stratified by treatment group; and represented on a logarithmic scale. Blood was drawn immediately prior to- and 5 mins following ICB administration. (**b**) Using only blood drawn prior to ICB infusion, the levels of anti-drug antibodies (ECL, electrochemiluminescence) were quantified by MSD assay, which were utilized to calculate the percentage of inhibition. Vertical arrows and dashed lines represent either an ICB infusion or ART interruption, as indicated, with the gray shaded area

representing ongoing ART. Individual RMs are indicated by shape with closed data points indicating animals with viral reactivation in plasma.

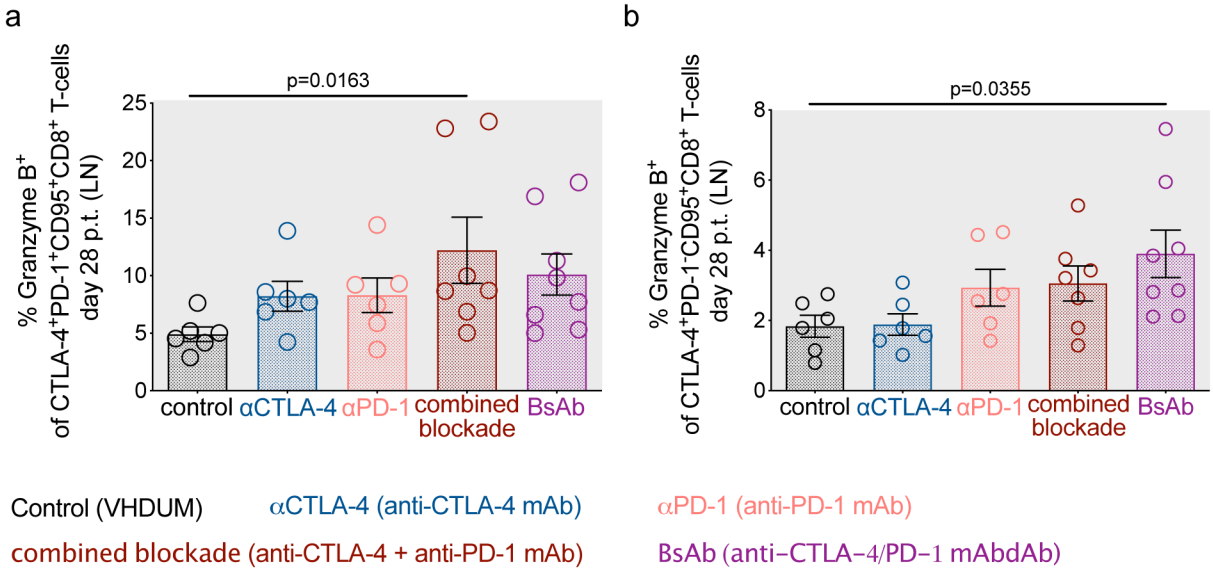

Extended Data Figure 4. Combined blockade leads to a limited restoration of cytolytic functionality in ICR-expressing CD8$^+$ T-cell subsets.

By flow cytometry, the frequencies of granzyme B$^+$ cells were determined within (**a**) CTLA-4$^+$PD-1$^+$ and (**b**) CTLA-4$^+$PD-1$^-$ memory CD8$^+$ T-cells in LN following the fourth ICB infusion (d28 p.t.). All RMs are color-coded and grouped based on ICB therapy with population sizes as indicated for all analyses: controls (n=6), black; αCTLA-4 (n=6), blue; αPD-1 (n=6), pink; combined blockade (n=7), red; and BsAb (n=8), purple. Averaged data are presented as the mean ± SEM and were analyzed with a two-sided Kruskal-Wallis test with Dunn's correction for multiple comparisons relative to controls.

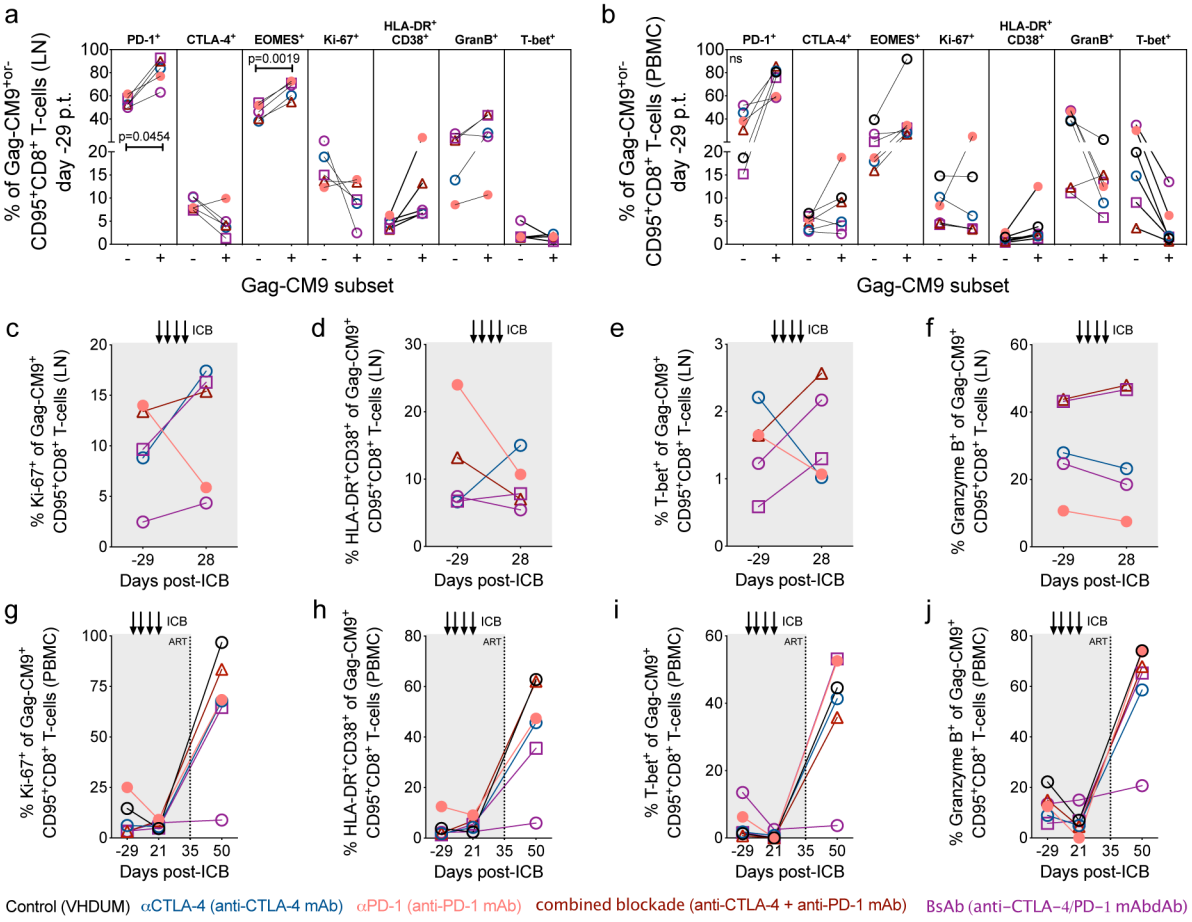

Extended Data Figure 5. SIV-specific CD8$^+$ T-cells display an exhausted phenotype that is not rescued by ICB during suppressive ART, but by viral rebound following ATI.

Within memory CD8$^+$ T-cells at the on-ART, pre-treatment baseline (d-29 p.t.; n=5 ICB-treated, *Mamu*-A*01$^+$ RMs) the frequencies of exhaustion, proliferative and activation biomarkers (as indicated above) were quantified via flow cytometry in SIV-specific and non-specific subsets, as assessed by anti-Gag-CM9 staining (as indicated below) in (**a**) LN and (**b**) PBMCs. Likewise, within LN SIV-specific memory CD8$^+$ T-cells the frequencies of (**c**) Ki-67$^+$, (**d**) HLA-DR$^+$CD38$^+$, (**e**) T-bet$^+$, and (**f**) Granzyme B$^+$ cells were measured at the pre-ICB baseline and following the fourth ICB infusion (d28 p.t.). Likewise, the frequencies of (**g**) Ki-67$^+$, (**h**) HLA-DR$^+$CD38$^+$, (**i**) T-bet$^+$, and (**j**) Granzyme B$^+$ cells within SIV-specific memory CD8$^+$ T-cells in PBMCs were quantified at the pre-ICB baseline, following the third ICB treatment (d21 p.t.), and 15 days following ART interruption (d50 p.t.). Analyses were conducted in up to 6 *Mamu*-A*01$^+$ RMs (**g,h,i,j**), of which 5 were ICB-treated (**a,b,c,d,e,f**). Each data point represents an individual animal, as indicated by shape, and those with ICB-related viral reactivation in plasma are represented as closed data points. Averaged data are presented as the mean ± SEM and were analyzed with (**a,b**) a one-way, pair-wise ANOVA using a Bonferroni correction for multiple corrections.

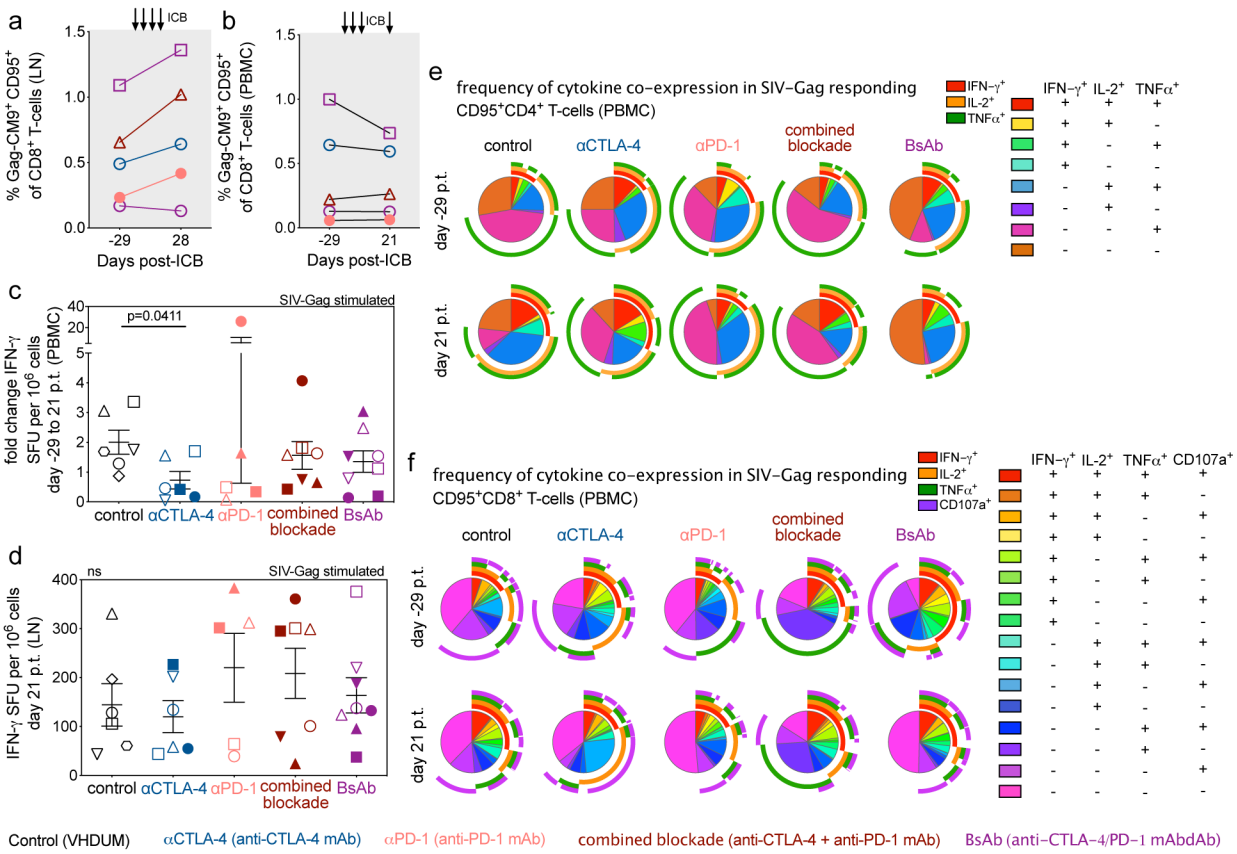

Extended Data Figure 6. SIV-specific CD8$^+$ T-cell responses are not enhanced by blockade of PD-1 and/or CTLA-4 during long-term ART.

In 5 *Mamu*-A*01$^+$, ICB-treated RMs, the frequency of SIV-specific cells, as determined via anti-Gag-CM9 tetramer staining with flow cytometry, were measured in (**a**) LN and (**b**) PBMC memory CD8$^+$ T-cells at treatment baseline (d-29 p.t.) and following ICB (d21 or 28 p.t.). The number of interferon gamma (IFN-γ) spot forming units (SFU) per 10^6 mononuclear cells were quantified by ELISpot upon SIV-Gag stimulation in (**c**) PBMCs as a fold-change (d21 p.t. relative to d-29 p.t.) and (**d**) cross-sectionally in LN (d21 p.t). Points represent unique animals, as indicated by shape and fill, as an average of three replicates with DMSO background subtracted. All RMs are color-coded and grouped based on ICB therapy as follows with population sizes as indicated for all ELISpot analyses: controls (n=6), black; αCTLA-4 (n=6), blue; αPD-1 (n=5), pink; combined blockade (n=7), red; and BsAb (n=8), purple. From *ex vivo* SIV-Gag-stimulated PBMCs with unstimulated background subtracted, the distribution of cytokine co-expression was determined via flow cytometry in memory (**e**) CD4$^+$ and (**f**) CD8$^+$ T-cells before (d-29 p.t.) and during (d21 p.t.; indicated at left) ICB administration (indicated above). Rainbow-colored inner pie wedges represent each Boolean combination of cytokine co-expression (annotated at far right); whereas, the stacked, outer concentric rings overlap with pie wedges that are positive for that cytokine (indicated at middle right): IFN-γ$^+$, red; IL-2$^+$, orange; TNFα$^+$, green; and CD107a$^+$, purple. Population sizes for all cytokine analyses are as follows: controls (n=6), black; αCTLA-4 (n=6), blue; αPD-1 (n=6), pink; combined blockade (n=7), red; and BsAb

(n=8), purple. Averaged data are presented as the mean ± SEM, and were analyzed with a two-sided (**c,d**) Mann-Whitney U test or (**e,f**) a Permutation test.

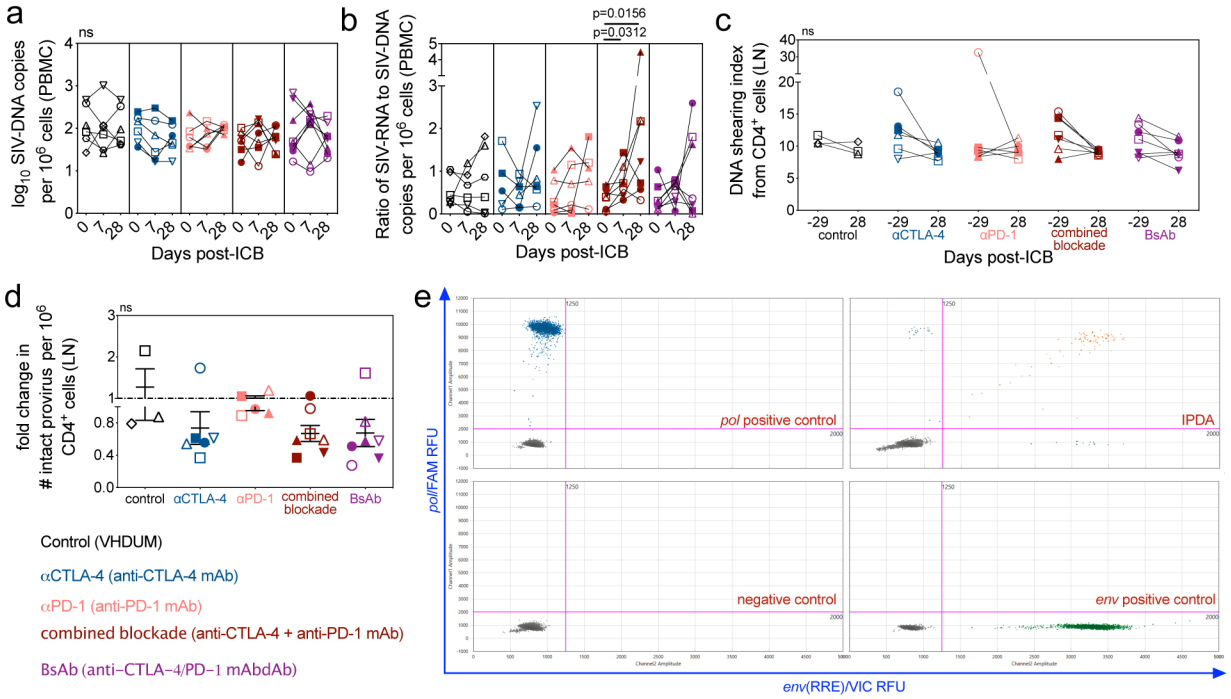

Extended Data Figure 7. Combined blockade increases the ratio of cell-associated SIV-RNA relative to SIV-DNA content in PBMCs and limit intact provirus in LN CD4$^+$ T cells.

(**a**) The number of log-transformed cell-associated SIV-DNA copies per 10^6 PBMCs were quantified by 12 replicate reaction RT-qPCR prior to the first infusion (d0 p.t.), and 1 week following the first (d7 p.t.) and fourth infusions (d28 p.t.); from which (**b**) the ratio of SIV-RNA to -DNA copies was computed. All RMs are color-coded and grouped based on ICB therapy as follows with population sizes as indicated for all RT-qPCR analyses: controls (n=6), black; αCTLA-4 (n=6), blue; αPD-1 (n=6), pink; combined blockade (n=7), red; and BsAb (n=8), purple. By IPDA with ddPCR, (**c**) the DNA shearing index pre- and post-ICB, and (**d**) the fold change in intact provirus per 10^6 cells relative to pre-treatment baseline were quantified in LN CD4$^+$ cells. For all IPDA analyses, population sizes are as follows: control (n=3), αCTLA-4 (n=6), αPD-1 (n=5), combined blockade (n=7), and BsAb (n=7). (**e**) An example IPDA plot is given for the amplification of the *env* relative response element (RRE) on VIC dye against *pol* on FAM dye in relative fluorescence units (RFU). A positivity cutoff of 1250 is used for *env* and 2000 for *pol*. Sample plots shown (as indicated in red) are as follows: negative control, merged analysis from no-template control and PBMCs at pre-infection from RLt16; *env* positive control, *env* gBlock (IDT); *pol* positive control, *pol* gBlock (IDT); and IPDA (shown are LN CD4$^+$ cells at d-29 p.t. from RWs16; 1 of 58 image sets of 8 replicate reactions). Averaged data are presented as the mean ± SEM. Each data point represents an individual animal, as indicated by shape, and those with ICB-related viral reactivation in plasma are represented as closed data points. Data were analyzed with a two-sided (**a,b**) Wilcoxon matched-pairs signed rank test, (**d**) a Mann-Whitney U test,

or (**c**) a two-way ANOVA with Bonferroni's correction for multiple comparisons relative to baseline and controls.

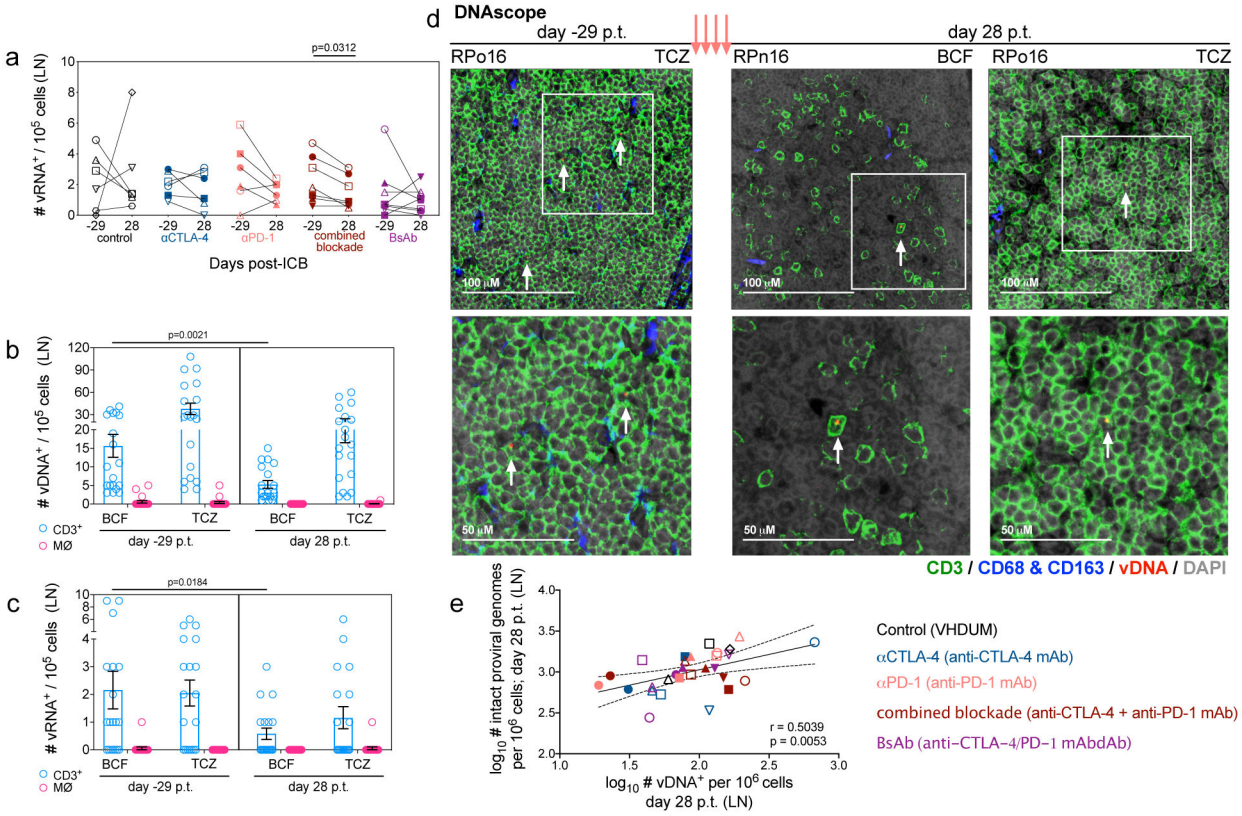

Extended Data Figure 8. ICB does not differentially impact viral reservoir content between lymphoid and myeloid lineages, and vDNA content correlates with intact proviral genomes.

(**a**) The number of LN vRNA$^+$ cells per 10^5 cells were quantified by RNAscope before (d-29) and after ICB therapy (d28 p.t.). All RMs are color-coded and grouped based on ICB therapy as follows with population sizes as indicated for RNAscope analyses: controls (n=6), black; αCTLA-4 (n=6), blue; αPD-1 (n=6), pink; combined blockade (n=7), red; and BsAb (n=8), purple. In the LN B-cell follicle (BCF) and T-cell zone (TCZ), the number of (**b**) vDNA or (**c**) vRNA cells per 10^5 cells were measured based on their co-expression of CD3 (lymphoid) or CD68/CD163 (MØ; myeloid) in a subset of ICB-responsive RMs (n=19). (**d**) *In situ* immunofluorescence staining for CD3 (green), CD68/CD163 (blue), and DAPI (grey) combined with hybridization for SIV vDNA (red) in LN TCZ or BCF (annotated at upper right) prior to or following ICB in representative RMs (3 of 38 unique samples; up to two tissue sections were analyzed). vDNA positive cells are annotated with a white arrow and successive magnification within the indicated boxed area (white) are shown below. (**e**) From LN at d28 p.t., the log-transformed frequency of vDNA$^+$ cells per 10^6 cells were correlated against the contemporaneous frequency of log-transformed intact proviral genomes per 10^6 CD4$^+$ cells (n=29). Averaged data are presented as the mean ± SEM and were analyzed with (**a,b,c**) a two-sided Wilcoxon matched-pairs signed rank test relative to baseline or (**e**) a Pearson correlation coefficient.

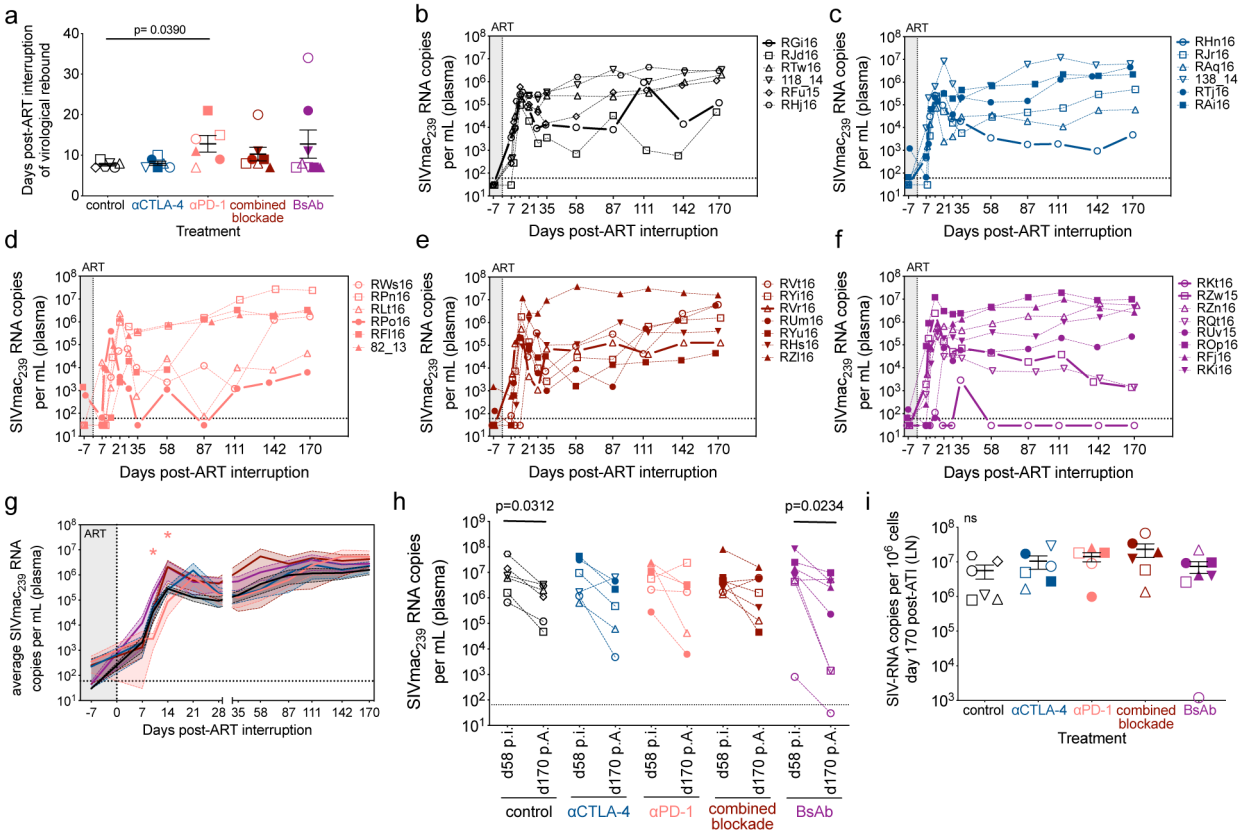

Extended Data Figure 9. Dual CTLA-4/PD-1 blockade does not control or delay viral rebound after ATI.

The delay in viral rebound by ICB was analyzed as the average number of days until detectable viral loads were observed in plasma with RT-qPCR. Plasma viral loads following ATI are shown for individual RMs by ICB: (**b**) control, (**c**) αCTLA-4, (**d**) αPD-1, (**e**) combined blockade, and (**f**) BsAb. *Mamu*-A*01^{+} RMs are shown with a bold connecting line and animals with prior ICB-related viral reactivation in plasma are represented as closed data points. The dashed horizontal line indicates the PCR assay limit of detection, with undetectable events plotted as 30 copies/mL. (**g**) Plasma viral loads following ATI were averaged by ICB and are shown with the mean as the solid line in bold and the SEM represented by the color-matched shaded region. (**h**) The attenuation in set point plasma viremia was analyzed between chronic infection (d52 p.i.) and following rebound (d170 post-ATI, p.A.). Population sizes are as follows for all viral load and rebound delay analyses: controls (n=6), black; αCTLA-4 (n=6), blue; αPD-1 (n=6), pink; combined blockade (n=7), red; and BsAb (n=8), purple. (**i**) By 12 replicate reaction RT-qPCR, the number of cell-associated SIV-RNA copies per 10^6 cells was quantified in axillary LN at necropsy: controls (n=6), αCTLA-4 (n=6), αPD-1 (n=5), combined blockade (n=6), and BsAb (n=7). Averaged data are presented as the mean ± SEM, and were analyzed with a two-sided (**g**) two-way ANOVA with Dunnett's correction for multiple comparisons or (**a,h,i**) a Mann-Whitney U test and/or Wilcoxon ranked sign test. Color-coded statistical asterisks indicate significance between control animals and the treatment group of that color. *, p<0.05; **, p<0.01; ***, p<0.001; ****, p<0.0001.

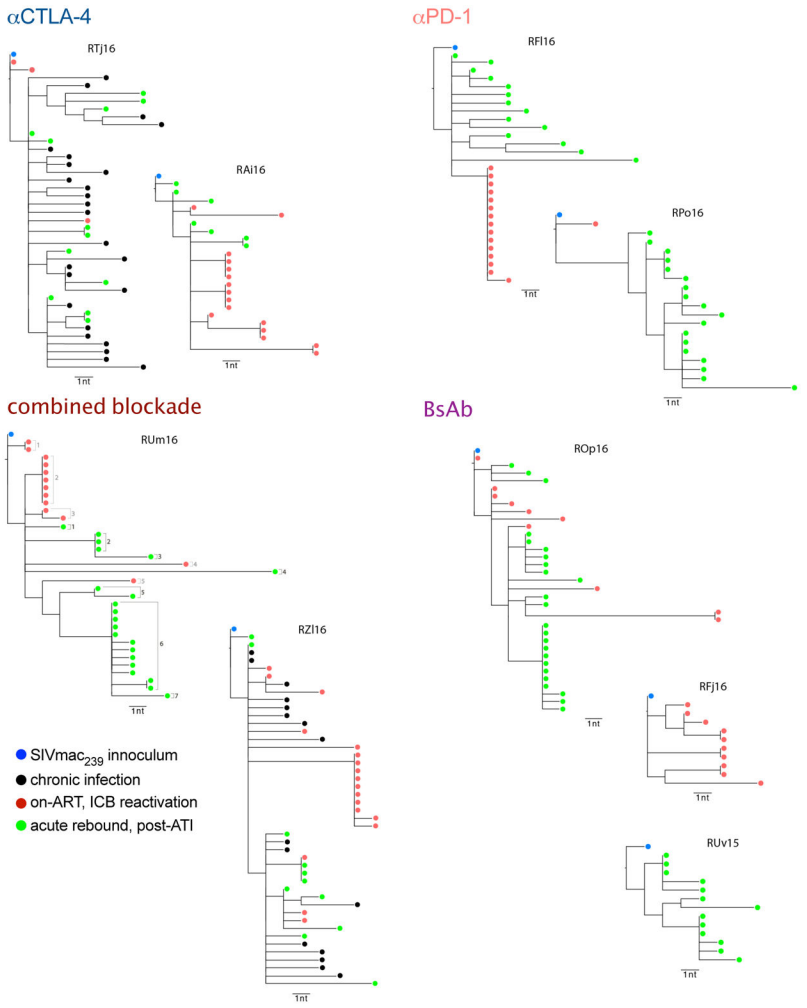

Extended Data Figure 10. Phylogenetic trees of gp160 *env* sequences from plasma.

Single genome sequencing-derived gp160 *env* sequences from the plasma of 9 RMs are displayed in maximum-likelihood phylogenetic trees. Virus obtained from different experimental phases are as follows: blue, $SIVmac_{239}$ inoculum; black, chronic infection prior to ART initiation (d52 p.i.); red, during on-ART ICB-mediated reactivation (d7-28 p.t.); and green, during acute rebound post-ATI. A scale bar indicating diversity for each phylogenetic tree is indicated below and lineage determinations are annotated for RUm16 (at right). Lineages were deemed distinct if they differed at 3 or more nucleotide positions over *env*.

Supplementary Material

Refer to Web version on PubMed Central for supplementary material.

Acknowledgments

We thank S. Ehnert, C. Souder, and E. Strobert (Research Resources and Veterinary Medicine) at YNPRC for providing animal and veterinary care, as well as the Emory Flow Cytometry Core. We thank C. Ashman, G. Jones, L. Anderson, and A. Barnard from GSK for assisting with the preparation and QC of the therapeutic antibodies, as

well as K. Fraley, A. Mayer, and G. Page from GSK for measuring antibody and anti-drug antibody levels. We would also like to thank R. Shoemaker, K. Oswald, and W. Bosche at Leidos Biomedical Research for technical assistance. The SIVmac239 strain used to infect the RMs was kindly provided by K. Van Rompay of UC-Davis; anti-Gag tetramers were provided by D. Long at the NIH Tetramer Core Facility at Emory; and ART was supplied through ViiV Healthcare and GSK. This work was supported by the NIAID, NIH under award numbers R01AI116379 and R21/R33AI116171 to M. Paiardini and by award UM1AI124436 (Emory CIAR). Support for this work was also provided by GlaxoSmithKline and Qura Therapeutics under subcontract 5105399; the Collaboratory of AIDS Researchers for Eradication (CARE; 1UM1AI126619-01) to D. Margolis; the Virology & Drug Discovery Core of Emory CFAR (P30AI050409); ORIP/OD award P51OD011132 (YNPRC) and P51OD011092 (ONPRC); and in part with federal funds from the National Cancer Institute, National Institutes of Health, under Contract No. HHSN261200800001E. The content of this publication does not necessarily reflect the views or policies of the Department of Health and Human Services, nor does mention of trade names, commercial products, or organizations imply endorsement by the U.S. Government.

Data Availability Statement

The data that support the findings of this study are available from the corresponding author on reasonable request. Sequences of gp160 *env* are available in GenBank (accession numbers MN856887 – MN857133).

References

1. McGary CS, et al. CTLA-4(+)PD-1(−) Memory CD4(+) T Cells Critically Contribute to Viral Persistence in Antiretroviral Therapy-Suppressed, SIV-Infected Rhesus Macaques. Immunity 47, 776–788 e775 (2017). [PubMed: 29045906]
2. Banga R, et al. PD-1(+) and follicular helper T cells are responsible for persistent HIV-1 transcription in treated aviremic individuals. Nat Med 22, 754–761 (2016). [PubMed: 27239760]
3. Fromentin R, et al. CD4+ T Cells Expressing PD-1, TIGIT and LAG-3 Contribute to HIV Persistence during ART. PLoS Pathog 12, e1005761 (2016). [PubMed: 27415008]
4. Perez VL, et al. Induction of peripheral T cell tolerance in vivo requires CTLA-4 engagement. Immunity 6, 411–417 (1997). [PubMed: 9133420]
5. Fife BT & Bluestone JA Control of peripheral T-cell tolerance and autoimmunity via the CTLA-4 and PD-1 pathways. Immunol Rev 224, 166–182 (2008). [PubMed: 18759926]
6. Perreau M, et al. Follicular helper T cells serve as the major CD4 T cell compartment for HIV-1 infection, replication, and production. J Exp Med 210, 143–156 (2013). [PubMed: 23254284]
7. Day CL, et al. PD-1 expression on HIV-specific T cells is associated with T-cell exhaustion and disease progression. Nature 443, 350–354 (2006). [PubMed: 16921384]
8. Trautmann L, et al. Upregulation of PD-1 expression on HIV-specific CD8+ T cells leads to reversible immune dysfunction. Nat Med 12, 1198–1202 (2006). [PubMed: 16917489]
9. Wightman F, et al. Effect of ipilimumab on the HIV reservoir in an HIV-infected individual with metastatic melanoma. AIDS 29, 504–506 (2015). [PubMed: 25628259]
10. Evans VA, et al. Programmed cell death-1 contributes to the establishment and maintenance of HIV-1 latency. AIDS 32, 1491–1497 (2018). [PubMed: 29746296]
11. Guihot A, et al. Drastic decrease of the HIV reservoir in a patient treated with nivolumab for lung cancer. Ann Oncol 29, 517–518 (2018). [PubMed: 29206889]
12. Scully EP, et al. Inconsistent HIV reservoir dynamics and immune responses following anti-PD-1 therapy in cancer patients with HIV infection. Ann Oncol 29, 2141–2142 (2018). [PubMed: 30032204]
13. Le Garff G, et al. Transient HIV-specific T cells increase and inflammation in an HIV-infected patient treated with nivolumab. AIDS 31, 1048–1051 (2017). [PubMed: 28350581]
14. Cecchinato V, et al. Immune activation driven by CTLA-4 blockade augments viral replication at mucosal sites in simian immunodeficiency virus infection. J Immunol 180, 5439–5447 (2008). [PubMed: 18390726]
15. Hryniewicz A, et al. CTLA-4 blockade decreases TGF-beta, IDO, and viral RNA expression in tissues of SIVmac251-infected macaques. Blood 108, 3834–3842 (2006). [PubMed: 16896154]

16. Velu V, et al. Enhancing SIV-specific immunity in vivo by PD-1 blockade. Nature 458, 206–210 (2009). [PubMed: 19078956]
17. Mylvaganam GH, et al. Combination anti-PD-1 and antiretroviral therapy provides therapeutic benefit against SIV. JCI Insight 3(2018).
18. Bekerman E, et al. PD-1 Blockade and TLR7 Activation Lack Therapeutic Benefit in Chronic Simian Immunodeficiency Virus-Infected Macaques on Antiretroviral Therapy. Antimicrob Agents Chemother 63(2019).
19. Wang C, et al. In vitro characterization of the anti-PD-1 antibody nivolumab, BMS-936558, and in vivo toxicology in non-human primates. Cancer Immunol Res 2, 846–856 (2014). [PubMed: 24872026]
20. Hardtke S, Ohl L & Forster R Balanced expression of CXCR5 and CCR7 on follicular T helper cells determines their transient positioning to lymph node follicles and is essential for efficient B-cell help. Blood 106, 1924–1931 (2005). [PubMed: 15899919]
21. Velu V, et al. Induction of Th1-Biased T Follicular Helper (Tfh) Cells in Lymphoid Tissues during Chronic Simian Immunodeficiency Virus Infection Defines Functionally Distinct Germinal Center Tfh Cells. J Immunol 197, 1832–1842 (2016). [PubMed: 27481845]
22. Pearce EL, et al. Control of effector CD8+ T cell function by the transcription factor Eomesodermin. Science 302, 1041–1043 (2003). [PubMed: 14605368]
23. Chen Z, et al. TCF-1-Centered Transcriptional Network Drives an Effector versus Exhausted CD8 T Cell-Fate Decision. Immunity (2019).
24. Fromentin R, et al. PD-1 blockade potentiates HIV latency reversal ex vivo in CD4(+) T cells from ART-suppressed individuals. Nat Commun 10, 814 (2019). [PubMed: 30778080]
25. Estes JD, et al. Defining total-body AIDS-virus burden with implications for curative strategies. Nat Med 23, 1271–1276 (2017). [PubMed: 28967921]
26. Bender AM, et al. The Landscape of Persistent Viral Genomes in ART-Treated SIV, SHIV, and HIV-2 Infections. Cell Host Microbe 26, 73–85 e74 (2019). [PubMed: 31295427]
27. Deleage C, et al. Defining HIV and SIV Reservoirs in Lymphoid Tissues. Pathog Immun 1, 68–106 (2016). [PubMed: 27430032]
28. Bar KJ, et al. Effect of HIV Antibody VRC01 on Viral Rebound after Treatment Interruption. N Engl J Med 375, 2037–2050 (2016). [PubMed: 27959728]
29. Amancha PK, et al. In vivo blockade of the programmed cell death-1 pathway using soluble recombinant PD-1-Fc enhances CD4+ and CD8+ T cell responses but has limited clinical benefit. J Immunol 191, 6060–6070 (2013). [PubMed: 24227774]
30. Dyavar Shetty R, et al. PD-1 blockade during chronic SIV infection reduces hyperimmune activation and microbial translocation in rhesus macaques. J Clin Invest 122, 1712–1716 (2012). [PubMed: 22523065]
31. Finnefrock AC, et al. PD-1 blockade in rhesus macaques: impact on chronic infection and prophylactic vaccination. J Immunol 182, 980–987 (2009). [PubMed: 19124741]
32. Okoye AA, et al. Early antiretroviral therapy limits SIV reservoir establishment to delay or prevent post-treatment viral rebound. Nat Med 24, 1430–1440 (2018). [PubMed: 30082858]
33. Borducchi EN, et al. Publisher Correction: Antibody and TLR7 agonist delay viral rebound in SHIV-infected monkeys. Nature 564, E8 (2018). [PubMed: 30397346]
34. Weiss L, et al. Human immunodeficiency virus-driven expansion of CD4+CD25+ regulatory T cells, which suppress HIV-specific CD4 T-cell responses in HIV-infected patients. Blood 104, 3249–3256 (2004). [PubMed: 15271794]
35. Nilsson J, et al. HIV-1-driven regulatory T-cell accumulation in lymphoid tissues is associated with disease progression in HIV/AIDS. Blood 108, 3808–3817 (2006). [PubMed: 16902147]
36. Larkin J, et al. Combined Nivolumab and Ipilimumab or Monotherapy in Untreated Melanoma. N Engl J Med 373, 23–34 (2015). [PubMed: 26027431]
37. Hao C, et al. Efficacy and safety of anti-PD-1 and anti-PD-1 combined with anti-CTLA-4 immunotherapy to advanced melanoma: A systematic review and meta-analysis of randomized controlled trials. Medicine (Baltimore) 96, e7325 (2017). [PubMed: 28658143]

38. Koelzer VH, et al. Systemic inflammation in a melanoma patient treated with immune checkpoint inhibitors-an autopsy study. J Immunother Cancer 4, 13 (2016). [PubMed: 26981243]
39. Cook MR & Kim C Safety and Efficacy of Immune Checkpoint Inhibitor Therapy in Patients With HIV Infection and Advanced-Stage Cancer: A Systematic Review. JAMA Oncol 5, 1049–1054 (2019). [PubMed: 30730549]
40. Hansen SG, et al. Profound early control of highly pathogenic SIV by an effector memory T-cell vaccine. Nature 473, 523–527 (2011). [PubMed: 21562493]

Methods-only References

41. Del Prete GQ, et al. Short Communication: Comparative Evaluation of Coformulated Injectable Combination Antiretroviral Therapy Regimens in Simian Immunodeficiency Virus-Infected Rhesus Macaques. AIDS Res Hum Retroviruses 32, 163–168 (2016). [PubMed: 26150024]
42. Scott MJ, et al. 'In-Format' screening of a novel bispecific antibody format reveals significant potency improvements relative to unformatted molecules. MAbs 9, 85–93 (2017). [PubMed: 27786601]
43. Chhabra M, et al. Binding Proteins in World Intellectual Property Organization, Vol. A2 (ed. WO/2018/083087) (GlaxoSmithKline, 2018).
44. Micci L, et al. Interleukin-21 combined with ART reduces inflammation and viral reservoir in SIV-infected macaques. J Clin Invest 125, 4497–4513 (2015). [PubMed: 26551680]
45. Pallikkuth S, et al. Maintenance of intestinal Th17 cells and reduced microbial translocation in SIV-infected rhesus macaques treated with interleukin (IL)-21. PLoS Pathog 9, e1003471 (2013). [PubMed: 23853592]
46. Li H & Pauza CD CD25(+) Bcl6(low) T follicular helper cells provide help to maturing B cells in germinal centers of human tonsil. Eur J Immunol 45, 298–308 (2015). [PubMed: 25263533]
47. Li H, et al. Envelope residue 375 substitutions in simian-human immunodeficiency viruses enhance CD4 binding and replication in rhesus macaques. Proc Natl Acad Sci U S A 113, E3413–3422 (2016). [PubMed: 27247400]
48. Amara RR, et al. Control of a mucosal challenge and prevention of AIDS by a multiprotein DNA/MVA vaccine. Science 292, 69–74 (2001). [PubMed: 11393868]
49. Hansen SG, et al. Addendum: Immune clearance of highly pathogenic SIV infection. Nature 547, 123–124 (2017). [PubMed: 28636599]
50. Roederer M, Nozzi JL & Nason MC SPICE: exploration and analysis of post-cytometric complex multivariate datasets. Cytometry A 79, 167–174 (2011). [PubMed: 21265010]
51. Bruner KM, et al. A quantitative approach for measuring the reservoir of latent HIV-1 proviruses. Nature 566, 120–125 (2019). [PubMed: 30700913]
52. Policicchio BB, et al. Dynamics of Simian Immunodeficiency Virus Two-Long-Terminal-Repeat Circles in the Presence and Absence of CD8(+) Cells. J Virol 92(2018).
53. Salantes DB, et al. HIV-1 latent reservoir size and diversity are stable following brief treatment interruption. J Clin Invest 128, 3102–3115 (2018). [PubMed: 29911997]
54. Guindon S, et al. New algorithms and methods to estimate maximum-likelihood phylogenies: assessing the performance of PhyML 3.0. Syst Biol 59, 307–321 (2010). [PubMed: 20525638]

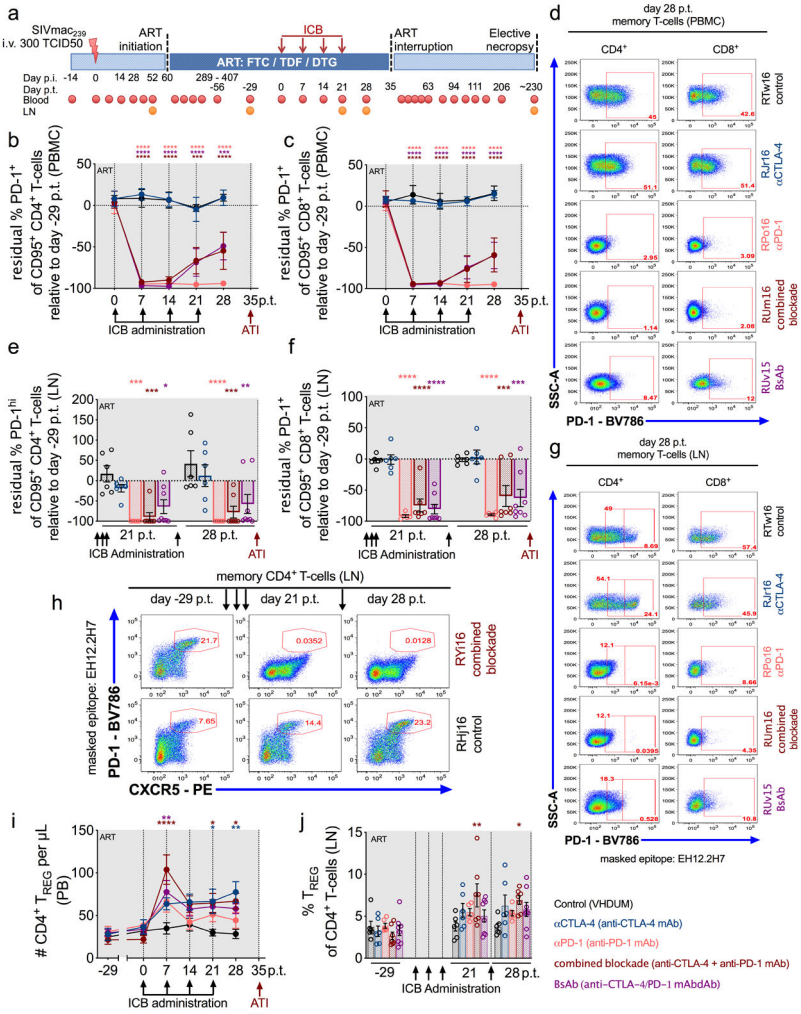

Figure 1. CTLA-4 and PD-1 blockade is biologically active in SIV-infected, ART-treated RMs.

(**a**) Study design; 34 RMs were infected i.v. with $SIVmac_{239}$, and at d60 p.i. initiated ART (FTC/DTG/TDF) that was maintained for up to 13.5 months. RMs were weekly administered i.v. ICB therapy over four weeks, and ART was interrupted 2 weeks afterwards with a 7 month follow up. PB and LN biopsies were collected at the specified time points. The frequency of residual PD-1 expression upon mAb occupancy relative to baseline (d-29 p.t.) was longitudinally quantified at the masked EH12.2H7 locus in memory $CD4^+$ and $CD8^+$ T-cells in PBMCs (**b,c**) and LN (**e,f**). Representative stains are shown for PD-1 occupancy in memory $CD4^+$ and $CD8^+$ T-cells (as indicated above; 5 of 33 single-replicate stains within each parent per tissue) in (**d**) PBMCs and (**g**) LN. (**h**) Representative stains are shown for PD-1 occupancy against CXCR5 expression within LN memory $CD4^+$ T-cells over time by ICB treatment (at right; 6 of 99 single-replicate stains). The number and frequency of $CD4^+$ T_{REGS} ($CD95^+CD25^+CD127^-FoxP3^+$) were quantified in (**i**) PB and (**j**) LN, respectively. RMs are color-coded and grouped based on ICB therapy as follows with population sizes as indicated for all analyses: vehicle/dummy (VHDUM) mAbdAb (controls; n=6), black; anti-CTLA-4 mAb (αCTLA-4; n=6), blue; anti-PD-1 mAb (αPD-1; n=6), pink; anti-CTLA-4 plus anti-PD-1 mAb (combined blockade; n=7), red; and anti-

CTLA-4/PD-1 mAbdAb (BsAb; n=8), purple. All averaged data are presented as the mean ± SEM, and were analyzed (**b,c,e,f,i,j**) with a two-sided, mixed-effects model with Dunnett's correction for multiple comparisons relative to controls. Color-coded statistical asterisks indicate significance between controls and the treatment group of the respective color. *, $p<0.05$; **, $p<0.01$; ***, $p<0.001$; ****, $p<0.0001$.

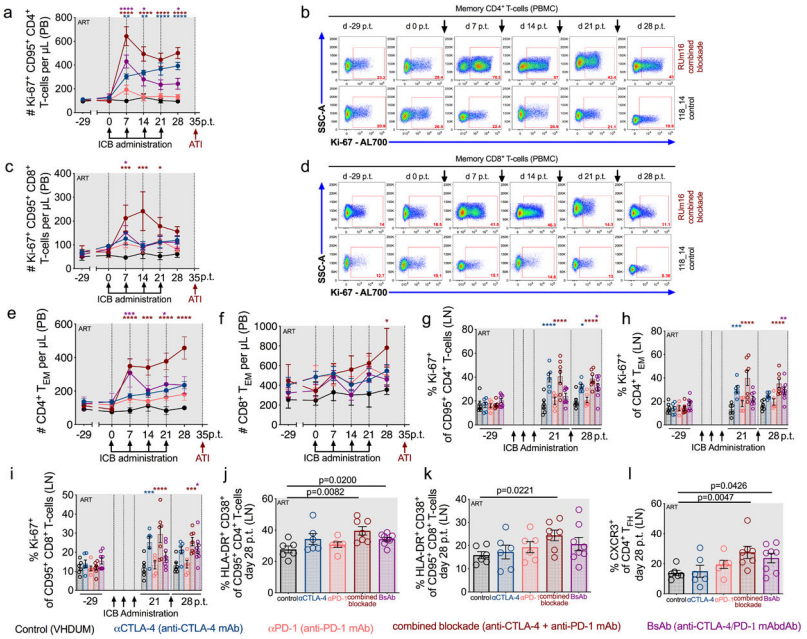

Figure 2. T-cell proliferative and effector responses are synergistically improved by dual CTLA-4/PD-1 blockade.

The number of cycling (Ki-67$^+$) memory (**a**) CD4$^+$ and (**c**) CD8$^+$ T-cells per μL of PB were measured and representative longitudinal stains are shown within memory (**b**) CD4$^+$ and (**d**) CD8$^+$ T-cells segmented by ICB (as indicated at right; RUm16 and 118_14 are shown as 12 of 198 single-replicate stains within each parental population). The number of (**e**) CD4$^+$ and (**f**) CD8$^+$ effector-memory cells (T_{EM}; CD95$^+$CCR7$^-$) per μL of PB were quantified longitudinally as was the frequency of cycling cells in LN (**g**) memory CD4$^+$, (**h**) CD4$^+$ T_{EM}, and (**i**) memory CD8$^+$ T-cells. Following ICB (d28 p.t.), the frequency of immune activation (HLA-DR$^+$CD38$^+$) was quantified in LN (**j**) memory CD4$^+$ and (**k**) memory CD8$^+$ T-cells, in addition to (**l**) the frequency CXCR3$^+$ CD4$^+$ T_{FH} (CXCR5$^+$PD-1^{hi}CD95$^+$). Individual animals are represented by open circles. All RMs are color-coded and grouped based on ICB therapy as follows with population sizes as indicated for all analyses: controls (n=6), black; αCTLA-4 (n=6), blue; αPD-1 (n=6), pink; combined blockade (n=7), red; and BsAb (n=8), purple. All averaged data are presented as the mean ± SEM, and were analyzed with (**a,c,e,f,g,h,i**) a two-sided, mixed-effects model with Dunnett's correction for multiple comparisons relative to controls or (**j,k,l**) a Mann-Whitney U test. Color-coded statistical asterisks indicate significance between control animals and the treatment group of that color. *, p<0.05; **, p<0.01; ***, p<0.001; ****, p<0.0001.

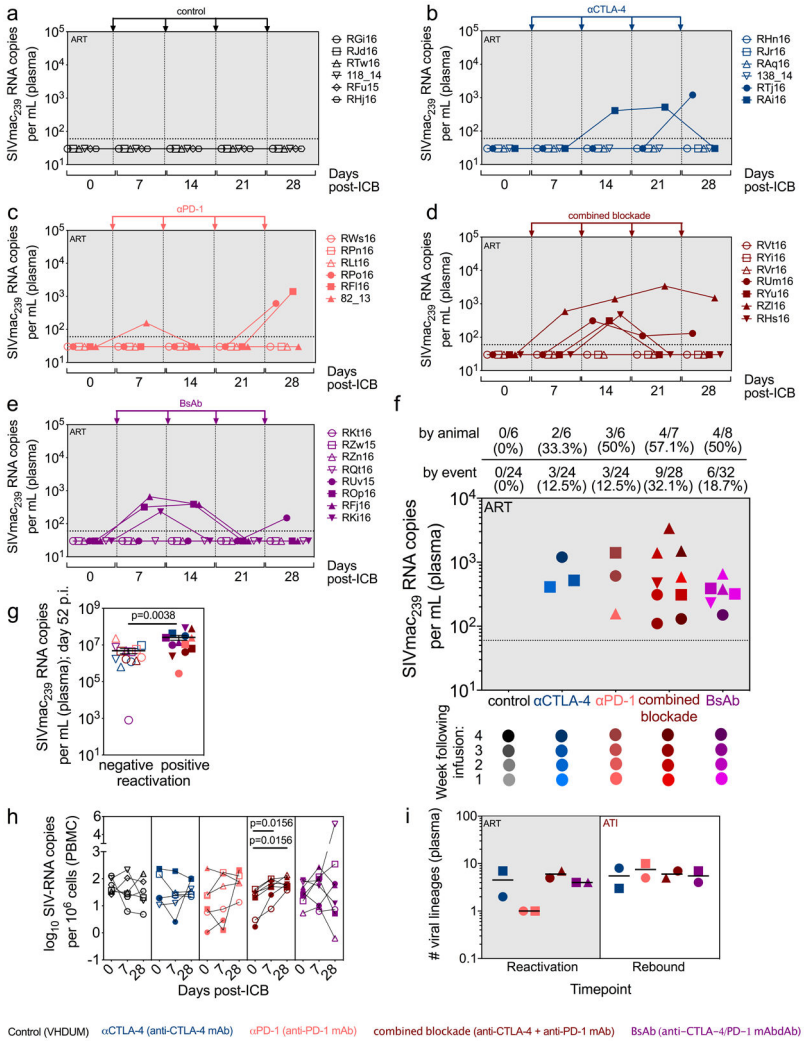

Figure 3. CTLA-4 and PD-1 combined blockade induces robust viral reactivation in ART-treated, SIV-infected RMs.

Single animal viral loads ($SIVmac_{239}$ RNA copies per mL of plasma) were quantified during ICB therapy on-ART immediately prior to each infusion, and 1 week following the terminal dose. Viral loads are segmented by treatment: (**a**) control (n=6), (**b**) αCTLA-4 (n=6), (**c**) αPD-1 (n=6), (**d**) combined blockade (n=7), and (**e**) BsAb (n=8). The hashed horizontal line indicates the assay limit of detection (≤60 copies/mL) with undetectable events plotted as 30 copies/mL. The x-axis is not drawn to scale; wherein, single time points have been spread and are grouped between hashed lines (as indicated below). (**f**) Treatment-grouped reactivation events (>60 copies/mL) are displayed on a logarithmic scale. Progressive color shading indicates after which infusion (number 1, 2, 3, or 4) the event followed (day 7, 14, 21, or 28 p.t., respectively), and individual animals are indicated by shape. The frequency and number of reactivation events is given relative to the number of animals and the total number of assayed events per treatment (as indicated above). (**g**) The set point plasma viral load (d52 p.i.) was stratified by subsequent viral reactivation in plasma (positive, n=13; negative, n=14). (**h**) The number of log-transformed cell-associated SIV-RNA copies per 10^6 cells in bulk PBMCs were quantified by 12 replicate reaction qPCR and segmented by

treatment: control (n=6), αCTLA-4 (n=6), αPD-1 (n=6), combined blockade (n=7), and BsAb (n=8). (**i**) The number of viral lineages, as determined by sequencing of gp160 *env*, in plasma that reactivated on-ART during ICB (left; 'Reactivation', n=8) and during early rebound post-ATI (right; 'Rebound', n=8) are shown. Viral lineages were deemed distinct if they differed by three or more nucleotide polymorphisms over gp160 *env* sequences. Individual RMs are indicated by shape with closed data points indicating viral reactivation in plasma. Averaged data are presented as the mean ± SEM, and were analyzed using a two-sided (**h**) Wilcoxon matched-pairs signed rank test or (**g**) Mann-Whitney U test.

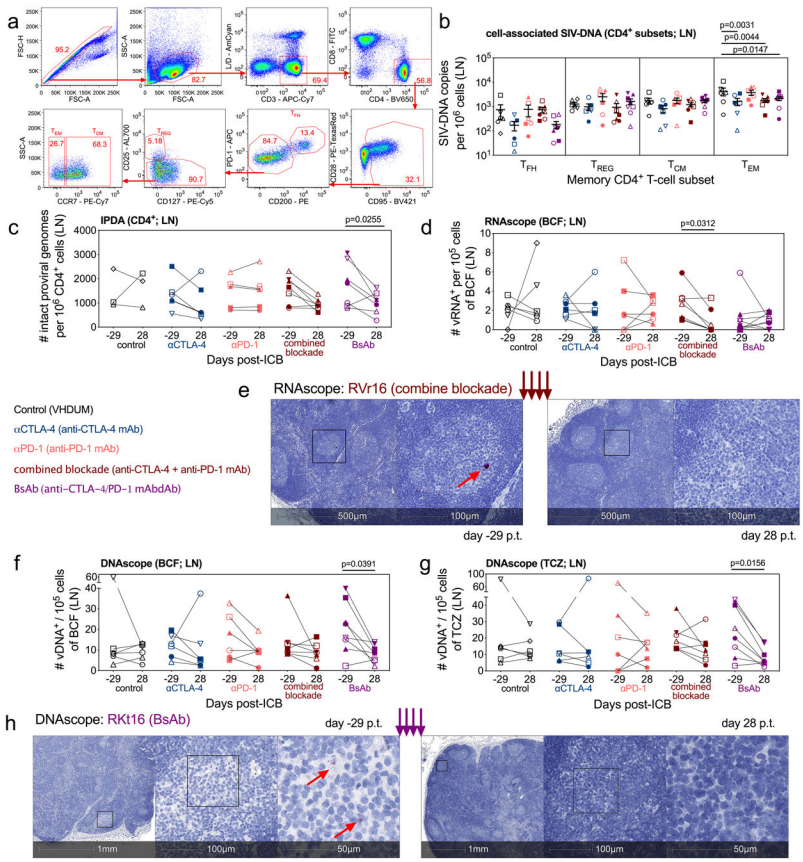

Figure 4. CTLA-4 and dual blockade, but not PD-1 blockade, reduces the total and intact SIV-DNA in LN.

In LN, memory subsets in CD4$^+$ T-cells were sorted at d28 p.t., (**a**) as shown in this representative gating strategy (1 of 33 single-replicate runs; RTj16), and (**b**) the cell-associated SIV-DNA content was determined via 12 replicate reaction RT-qPCR. Within the memory CD4$^+$ T-cells, the sorted populations are defined as follows: T_{FH}, PD-1^{hi}CD200^{hi}; T_{REG}, PD-1^{lo}CD200^{lo}CD127$^-$CD25$^+$; T_{CM}, PD-1^{lo}CD200^{lo}CD25$^-$CCR7$^+$; and T_{EM}, PD-1^{lo}CD200^{lo}CD25$^-$CCR7$^-$. (**c**) By 8 replicate reaction IPDA, the number of intact proviral genomes per 10^6 CD4$^+$ cells were quantified in LN at pre-treatment baseline (d-29 p.t.) and following the fourth ICB (d28 p.t.): control (n=3), αCTLA-4 (n=6), αPD-1 (n=6), combined blockade (n=7), and BsAb (n=7). (**d**) By RNAscope, the number of vRNA$^+$ cells per 10^5 cells were measured in the lymphoid B-cell follicle (BCF) and (**e**) a representative stain is shown for vRNA (red) in the LN BCF both pre- and post-treatment (combined blockade-treated RVr16; 1 of 33 unique samples quantified from up to two tissue sections). Distance scale is given below each panel with successive magnifications within the indicated area (black square) extending to the right. By DNAscope the number of vDNA$^+$ cells per 10^5 cells were quantified in the lymphoid (**f**) BCF and (**g**) the T-cell zone (TCZ). (**h**) A representative stain (BsAb-treated RKt16; 1 of 33 unique samples quantified from up to two tissue sections) is shown for vDNA (red). For all analyses, except IPDA as indicated, annotations and population sizes are as follows: controls (n=6), black; αCTLA-4 (n=6), blue; αPD-1 (n=6), pink; combined blockade (n=7), red; and BsAb (n=8), purple. Individual RMs are indicated by shape with closed data points indicating viral reactivation in plasma.

Averaged data are presented as the mean ± SEM, and were analyzed with a two-sided two-way ANOVA or mixed-effect model with (**b**) Dunnett's correction relative to controls or (**c**) Bonferroni's corrections for multiple comparisons relative to baseline, or (**d,f,g**) a Wilcoxon matched-pairs signed rank test.